eScience 4 (2024) 100243

Contents lists available at ScienceDirect

eScience

journal homepage: www.keaipublishing.com/en/journals/escience

Review

Managing the lifecycle of perovskite solar cells: Addressing stability and environmental concerns from utilization to end-of-life

Hee Jung Kim [a], Gill Sang Han [b,*], Hyun Suk Jung [a,c,*]

[a] School of Advanced Materials Science & Engineering, Sungkyunkwan University, 2066, Seobu-ro, Jangan-gu, Suwon-si, Gyeonggi-do 16419, Republic of Korea
[b] Division of Advanced Materials, Korea Research Institute of Chemical Technology (KRICT), Daejeon 34114, Republic of Korea
[c] SKKU Institute of Energy Science and Technology (SIEST), Sungkyunkwan University, Suwon 16419, Republic of Korea

HIGHLIGHTS

- We have summarized the challenges and recent research associated with the lifecycle of perovskite solar cells (PSCs).
- Key stability strategies, including the use of additives and interfacial layers, are outlined.
- We reviewed methods for extending the lifetime of PSCs and improving their stability.
- Crucial recycling strategies for noble and toxic materials, along with related challenges, are discussed.

GRAPHICAL ABSTRACT

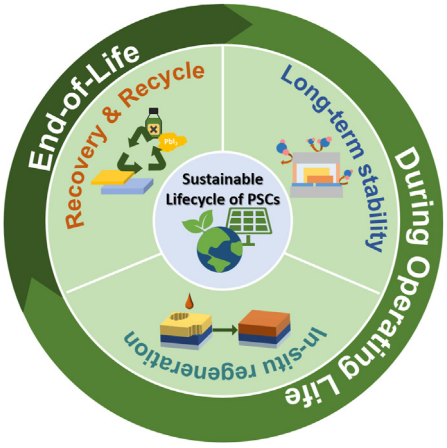

Abbreviations: AgI, silver iodide; AR, anti-reflection; a-PVKD, alkylated amorphous perovskitoid; BzA, benzyl acrylate; c-PVK, crystalline perovskite; ChCl, choline chloride; CIGS, copper indium gallium selenide; CTL, charge transport layer; CuI, copper iodide; DES, deep eutectic solvent; Di-G, diphosphatidyl-glycerol; DMF, *N,N*-Dimethylformamide; DMIMB, 1-decyl-3-methylimidazolium bromide; EG, ethylene glycol; [EMIM]Br, 1-ethyl-3-methylimidazolium bromide; ETL, electron transport layer; Fc, ferrocene; CDA, 4,4′-carbonyldiphthalic anhydride; FDA, 4,4′-(hexafluoroisopropylidene)diphthalic anhydride; 4TA, 4-[(trifluoromethyl) sulfonyl]-aniline; Hap, hydroxyapatite; HTM, hole transport material; IL, ionic liquid; LCA, lifecycle assessment; LCOE, levelized cost of electricity; MAI, methylammonium iodide; NDI, 1,5-naphthalene diisocyanate; 1,2-EDT, 1,2-ethandeithiol; PBAT, poly(butyleneadipate-coterephthalate) polymer; PCE, power conversion efficiency; $PDEAI_2$, (phenylene)di(ethylammonium) iodide; PDMS, polydimethylsiloxane; PEG, polyethylene glycol; PIB, polyisobutylene; PLL, poly-L-lysine; PLLS, sulfonic-acid-modified poly-L-lysine; PMMA, polymethyl methacrylate; PO, polyolefin; PPFC, plasma-polymerized fluorocarbon; PSC, perovskite solar cell; PSM, perovskite solar module; PUDS, polyurethane elastomers with disulfide bonds; PV, photovoltaic; PVP, polyvinylpyrrolidone; RH, relative humidity; RoHS, Restriction of Hazardous Substances; S-GA, sulfonated graphene aerogels; SHP, polysiloxane; SiSH, 3-mercaptopropyltriethoxysilane; Spiro-OH, 2,2′,2″,2‴-(((9,9′-spirobi[fluorene]-2,2′,7,7′ tetrayltetrakis(phe-nylazanediyl))tetrakis(ethane-2,1-diyl))tetr-akis(oxy))tetrakis(-ethan-1-ol); TCO, transparent conductive oxide; WEEE, waste electrical and electronic equipment; ZnP, zinc porphyrin.

* Corresponding authors.
E-mail addresses: gshan@krict.re.kr (G.S. Han), hsjung1@skku.edu (H.S. Jung).

https://doi.org/10.1016/j.esci.2024.100243
Received 1 September 2023; Received in revised form 8 December 2023; Accepted 22 January 2024
Available online 25 January 2024

ARTICLE INFO

Keywords:
Levelized cost of electricity
Metal electrode
Pb leakage
Perovskite
Power conversion efficiency
Solar cell life cycle

ABSTRACT

Perovskite solar cells (PSCs) have shown remarkable advancements and achieved impressive power conversion efficiencies since their initial introduction in 2012. However, challenges regarding stability, quality, and sustainability must be addressed for their successful commercial use. This review analyses the recent studies and challenges related to the operating life and end-of-life utilization of PSCs. Strategies to enhance the stability and mitigate the toxic Pb leakage in operational and recycling approaches of discarded PSCs post their end-of-life are examined to establish a viable and sustainable PSC industry. Additionally, future research directions are proposed for the advancements in the PSC industry. The goal is to ensure high efficiency as well as economic and environmental sustainability throughout the lifecycle of PSCs.

1. Introduction

Global population growth and rapid industrial development have resulted in an increasing demand for sustainable energy worldwide. Among the various renewable energy sources (namely water, wind, biomass, and solar power), solar energy is the most promising because it is inexhaustible, clean, and long-lasting. PSCs have shown significant advancements since their initial introduction [1], achieving an impressive 26% PCE [2]. This progress has been driven by research focusing on high efficiency, modularization, and reproducibility of PSCs, bringing them closer to commercialization. However, certain challenges, particularly those concerning quality assurance and sustainability, must be addressed. In addition to achieving high efficiency, ensuring economic and environmental sustainability during the entire PSC lifecycle is essential.

When evaluating energy sources, LCOE is a commonly used metric that considers efficiency, cost, and lifetime. Despite their low initial cost, PSCs have an LCOE of ~14 US cents/kW/h owing to their shorter lifetime (~1 y) [3,4], which is higher than those of other PV technologies including Si, CIGS, and CdTe solar cells (3–5 US cents/kW/h) [3]. To compete with commercial Si solar cells, PSCs must last for at least 16 y, assuming at 25% PCE [5]. Therefore, extending their operational lifetime is crucial for successful commercialization. The PSC lifetime is influenced by intrinsic and extrinsic stability factors [6]. Enhancing the extrinsic stability through encapsulation techniques protects PSCs from external factors including moisture and oxygen. However, intrinsic stability is still limited by heat, light, and bias due to the presence of numerous defects in the perovskite film.

PSCs also contain toxic Pb components within the perovskite material, which may leak during exposure to external stimuli (such as high temperature, humidity, and intense light) and cause environmental and health risks. Consequently, the use of Pb in Europe is restricted to 0.1% according to the RoHS Directive [7]. Efforts such as inner passivation and encapsulation have been made to reduce Pb leakage during PSC operation; however, it is equally essential to properly manage the discarded PSCs and handle the toxic Pb and precious materials post their end-of-life. Recently, LCAs have highlighted the significance of recycling strategies, proving that they are more economically and environmentally effective than landfill options [8]. Implementing recycling strategies is therefore crucial for achieving a sustainable and eco-friendly PSC industry while responsibly managing the toxic substances and precious materials.

This review addresses the challenges and recent studies pertaining to two main aspects of PSCs: their performance during operating life and end-of-life utilization (Fig. 1). First, we examine various strategies aimed at enhancing stability and mitigating Pb leakage during operation. Next, we explore recent recycling approaches for discarded post-end-of-life PSCs to establish a viable and sustainable PSC industry. Finally, we propose research directions and offer perspectives for advancing the construction of the PSC industry.

2. PSC structures and working principle

The structure of PSCs is a simple stack structure, illustrated in Fig. 2a. This involves incorporating perovskite material as a light-absorbing layer between two electrodes. To mitigate carrier losses resulting from the work function difference between the electrode and the light-absorbing layer, a carrier transport layer (CTL) is introduced between the light-absorbing layer and the electrode. Initially, electron-hole pairs are generated when light is introduced into the absorber layer, which is composed of perovskite materials with an ABX_3 structure (Figs. 2b–d). In general, A and B denotes monovalent organic materials (MA^+, FA^+) and Pb^{2+} or Sn^{2+}, respectively, and halide atoms including I, Cl, Br, and etc. are used for X cites. The optical properties of perovskite can be tuned by varying either monovalent cation or the halide components, suggesting the wider solar cell applications [9–11]. The generated electrons and holes then transferred to front and back electrodes, respectively, through the CTL. The thin layer of n-type materials is usually introduced as ETL, whereas p-type materials served as HTL. The ETL assists the generated electrons transferred to the front electrodes, also blocking release of holes towards to front electrode. The n-type materials such as TiO_2, ZnO, SnO_2, and PCBM are widely used due to its higher electron affinity and ionization potential. Then the electrodes are gathered at front electrodes. The front electrodes require several properties including good electrical conductivity, high transmittance, and high work function, thus FTO and ITO are widely employed. On the other hand, the hole transferred to back electrodes through the HTL, the p-type materials such as Spiro-OMeTAD (2,20,7,70-tetrakis-(*N*,*N*-di-p-methoxyphenylamine)-9, 90-spiro-biuorene), P3HT (Poly(3-hexylthiophene-2,5-diyl)), and CuI. The back electrodes include Al, Ag, Au, Cu, and Pt that are stable and have low work function. The PSC structures are classified based on their layered configuration, leading to distinct pathways for light. In the conventional (n–i–p) structure, light progresses through TCO and subsequently the ETL. In contrast, the inverted (p–i–n) structure allows light to pass through the TCO and then the HTL, as illustrated in Figs. 2a and c. While the conventional PSC was initially reported and achieved a certified efficiency above 25% [12–15], it presents challenges such as high hysteresis and low stability, leading to a shortened lifetime [16,17]. Consequently, the inverted PSC has garnered more attention due to several advantages, including low hysteresis, high stability, and a simpler process [18–20]. Despite this, the efficiency gap between conventional and inverted PSCs highlights the need for further study.

3. Operating life

Despite considerable advancements in efficiency, the practical use of PSCs as a next-generation energy source is hindered by their shortened lifetimes. Although PSCs are more cost-effective than Si solar cells, they display a significantly higher LCOE that is primarily attributed to their limited lifespans. Research has indicated that the LCOE of PSCs is approximately threefold higher than that of other solar cells [3], underscoring the urgency of extending their lifetime. Consequently, extensive efforts have been devoted toward enhancing the stability and regeneration processes to prolong the lifespan of PSCs. Moreover, toxic Pb generation and leakage during operating life not only impact the environment but also reduce the PSC stability. To address this issue, several studies have focused on Pb immobilization.

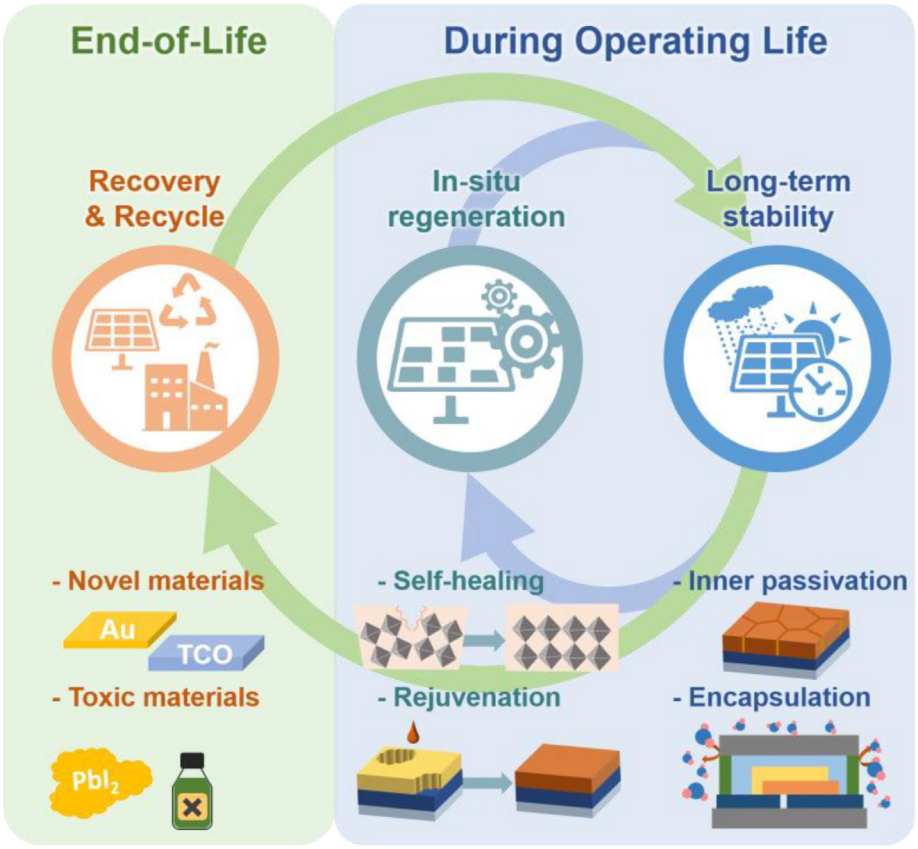

Fig. 1. Schematic illustration of sustainable PSCs lifecycle from utilization to end-of-life.

3.1. Stability

Numerous studies have extensively discussed PSC degradation and efforts to improve the PSC stability by considering both intrinsic and extrinsic stability factors [21–24]. Intrinsic stability can be improved by optimization of metal electrodes, alleviation of internal stress, immobilizing the inner composition, whereas extrinsic stability is enhanced through encapsulation strategies that effectively block the penetration of external environmental factors, including water and oxygen. Additionally, several strategies have been proposed to prevent Pb leakage by immobilizing Pb, advocating an environmentally sustainable PSC industry.

3.1.1. Optimization of metal electrode

Metal electrodes pose a substantial challenge, compromising the stability of PSCs by inducing issues such as ion migration and reactions with the perovskite layer. Ag, commonly used as top metal electrode in PSCs, raises stability concerns due to its reaction with halides, leading to the formation of silver halides [25,26]. Au, another frequently employed metal electrode, is more stable than Ag; however, it carries the potential to diffuse toward the perovskite layer, resulting in the irreversible degradation of PSCs [27,28]. Therefore, alternative metals such as Cu, Ni, Mo, and W have been utilized as substitutes for Ag and Au electrodes [29–31]. A Cu electrode, investigated in PSCs, demonstrates excellent stability due to remarkable corrosion resistance [32–34]. Xu *et al.* recently achieved a PCE of 20.10% in Cu-based n–i–p PSCs, showcasing high stability by retaining 92% of their initial PCE after 1000 h of storage [35]. In the absence of oxygen and moisture, Cu remains stable even in direct contact with the perovskite layer, showing no diffusion of Cu into the perovskite after long-term annealing or sun illumination [36]. However, Cu can be oxidized in the presence of oxygen and moisture, and the resulting oxidation products can cause perovskite decomposition [36]. Additionally, Mo and Ni were utilized as electrodes and exhibited better stability compared with Ag electrodes [30]. In particular, the Mo electrode exhibited superior hardness and elasticity compared to Au, positioning Mo as a promising candidate for replacing noble metal electrodes [31]. Nevertheless, previous studies using alternative metal electrodes in PSCs revealed relatively low PCE, emphasizing the necessity for further research to improve photovoltaic performance. Carbon based electrodes have attracted attention in PSCs due to their high conductivity, tunable structures, and chemical stability [37,38]. In addition to metal electrodes, organic HTMs are considered as main factor for low stability, leading to an increased focus on HTM-free PSCs utilizing carbon electrodes (C-PSCs) [39–41]. However, despite achieving high stability, C-PSCs face challenges such as poor contact with the perovskite layer and low power conversion efficiency (PCE) [42,43]. The introduction of an HTM between the perovskite and carbon electrodes can enhance photovoltaic performance by facilitating efficient charge separation and hole collection. Recently, Du *et al.* developed hole-transporting bilayers (HTbL) for fully printed C-PSCs, achieving an enhanced PCE of 19.2% compared to C-PSCs fabricated with a single HTL [44]. Moreover, C-PSCs with HTbL exhibited no noticeable degradation even after 2500 h under 65 °C and one sun aging test, highlighting the considerable potential of carbon as an effective electrode in PSCs. Additionally, various strategies, such as incorporating polymers [45,46], multilayer electrodes [47–49], and introducing bilayers [27,50], have been employed to mitigate the decrease in stability caused by metal electrodes. However, additional studies are still required to further enhance photovoltaic performance for practical applications.

3.1.2. Inner passivation

PSC stability is attributed to various factors including ion migration, metal electrode corrosion, and residual strain, which are induced by operational conditions such as light, heat, and electric fields [3,22].

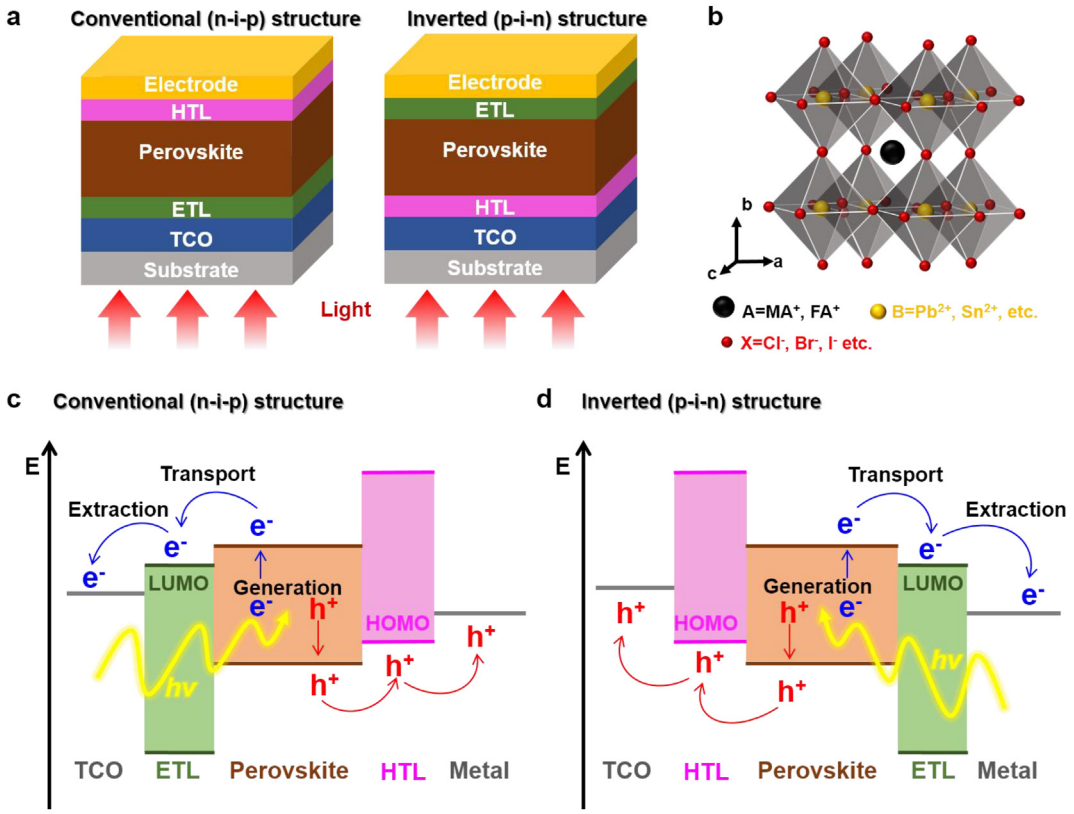

Fig. 2. Schematic illustration of (a) two distinct PSC structures and (b) the perovskite structure. The energy band diagram for (c) conventional and (d) inverted structure PSC.

Organic–inorganic hybrid perovskites lack chemical robustness owing to the weak ionic bonds and van der Waals interactions that bind their organic and inorganic components within the lattice structure, making them susceptible to decomposition when exposed to different stimuli [22,51]. Consequently, harsh conditions including light illumination, high operational temperature, and an electric field can disrupt the weak ionic bonds within the perovskite structure, leading to the migration of dissociated ions.

Spiro-OMeTAD, commonly used as the hole-transporting material (HTM) in PSCs, has been reported to undergo irreversible degradation when partially oxidized spiro-OMeTAD reacts with migrating I^- at the spiro-OMeTAD/perovskite interfaces [52]. Additionally, spiro-OMeTAD was found to generate iodine containing byproducts when exposed to moisture. These byproducts then diffused into the Ag electrode, accelerating the degradation of PSCs by forming AgI [25]. One potential solution to this issue involves introducing interfacial layers between the HTM and perovskite layer, thereby preventing ion migration.

Considering these challenges, numerous efforts have been made to enhance the stability by addressing the aforementioned issues (Table 1). Regarding ion migration, several studies have focused on incorporating additives that coordinate with the functional groups present in the perovskite components [23,53–58,61–63]. These additives have been utilized in perovskite precursors to immobilize ions in the perovskite structures. Niu *et al.* employed polymerizable additives (AAm monomers) containing carbonyl functional groups in the perovskite precursor to immobilize Pb ions by forming a polymerized network (Figs. 3a and b) [53]. Through thermal treatment, the AAm monomer was transformed into a Pb-chelating polymer, effectively preventing Pb leakage from the perovskite layer. Consequently, the PSCs exhibited enhanced stability, maintaining 80% of the initial PCE after 1000 h under one sun equivalent illumination, compared with the control PSCs that maintained 80% for 600 h under the same conditions (Fig. 3c). Other functional groups including fluorine [54], sulfonic [23,55], and carboxyl groups [58], have also been employed to immobilize Pb ions. These Pb-ion-immobilizing strategies enhance the stability of PSCs and reduce their environmental impact by effectively preventing Pb leakage. Management of organic cations is also crucial for achieving high PSC stability. Organic cations are particularly sensitive because of their weaker bonding with the Pb–I framework, making them more prone to bond breakage and migration that accelerate PSC decomposition [76]. Furthermore, the low activation energy of organic cations reduces the precursor quality, leading to the formation of the δ-phase perovskite [77]. Zhu *et al.* introduced Lewis bases that exhibited excellent interaction with Pb and formamidinium ($CH(NH_2)$) ions simultaneously in the perovskite precursor [56]. FDA molecules comprising ^{15}F in diphthalic anhydride, employed as Lewis bases, effectively passivated and enhanced the stability of both the perovskite precursor and PSCs, as shown in Fig. 3d. The PCE of PSCs fabricated with an FDA-added precursor increased to 22.43% (PCE of control PSCs, 19.58%) and retained ~90% of the initial PCE, even after 1000 h of heating at 80 °C (thermal) or exposure to 50% RH atmospheric testing, without the need for encapsulation (Figs. 3e and f). Meanwhile, the multifunctional molecule 4TA was employed in the perovskite precursor to enhance the operational stability of the perovskite by passivating surface defects [57]. 4TA has two functional groups: (1) The trifluoromethyl group forms hydrogen bonds with methylammonium ions, preventing organic cation defects and serving as a hydrophobic barrier to shield the perovskite surface from humidity exposure; and (2) the aniline group coordinates with uncoordinated Pb ions, effectively passivating ion defects and reducing Pb leakage. This approach significantly improved the operational stability—a long-term stability of 93% of the initial PCE was achieved after 30 d of storage in air (~55% humidity)—with a high PCE of 20.24% (Fig. 3g). Additionally, to passivate perovskite surface defects, additives were introduced into the antisolvent instead of being added to the perovskite precursor. Liang *et al.* dissolved ZnP in an antisolvent (methylbenzene) and subjected it to thermal polymerization to passivate the perovskite surface [61]. The

Table 1
Summary of various strategies for enhancing the stability by inner passivation.

Method	Passivation materials	PSC architectures	PCE (control PCE)	Stability (control stability) *Stability condition	Pb leakage (Pb leakage for control)	Module PCE (control) *Size	Ref.
Additive (perovskite precursor)	Polymerizable acrylamide (PAm)	Ag/BCP/PCBM/i-PAM/i-PAM@ $Cs_{0.05}(FA_{0.90}MA_{0.10})_{0.95}Pb(I_{0.90}Br_{0.10})_3$ /PTAA/NiO_x/ITO/glass	22.1% (best) (20.1%)	80% after 1000 h (80% after 600 h) *One sun illumination	1.33 ppm after immersed in water for 225 min (2.90 ppm)	15.7% *19.16 cm^2	[53]
	Fullerene–porphyrin dyad (FAD)	Ag/spiro-OMeTAD /FAD-$FA_{0.94}MA_{0.01}Cs_{0.05}Pb(I_{0.99}Br_{0.01})_3$ /SnO_2/ITO/glass	23.00% (best) 22.56% (aver.) (20.99%/20.36%)	>83% after 1500 h *Ambient air	~700 ppm after immersion in water for 90 s (~1200 ppm)	–	[54]
	Heptadecafluo-rooctanesulfonic acid tetraethylammonium salt (HFSTT)	Au/spiro-OMeTAD/ $(FAPbI_3)_{0.98}(FAPbBr_3)_{0.02}$(HFSTT) /$TiO_2$/FTO/glass	23.88% (best) (22.02%)	80% after 700 h (80% after 70 h) *60 °C, 60% RH	N/A	18.27% (16.91%) *60.68 cm^2	[23]
	Amphoteric phenylbenzimidazole sulfonic acid (PBSA)	Au/spiro-OMeTAD /$FA_{0.92}MA_{0.08}PbI_3$/SnO_2/ITO/glass	23.27% (best) (20.38%)	~85% after 1000 h (~40% after 1000 h) *Ambient air, 30% RH	<1 ppm after immersion in water for 250 min (~3.5 ppm)	15.31% *19.32 cm^2	[55]
	4,4′-(Hexafluoroisopropylidene) diphthalic anhydride (FDA)	Au/spiro-OMeTAD /$(FAPbI_3)_{0.95}(MAPbBr_3)_{0.05}$ /TiO_2/FTO/glass	22.43% (best) (19.58%)	88% after 600 h (38% after 200 h) *Ambient air, dark, 50% RH	N/A	–	[56]
	4-[(Trifluoromethyl) sulfonyl]aniline (4TA)	Ag/spiro-OMeTAD/$MAPbI_3$-4TA /SnO_2/ITO/glass	20.24% (best) (18.00%)	93% after 30 d *~55% RH	10 ppm after immersion in pH ~5.7 water for 60 s (50 ppm)	–	[57]
	Carbon nanotubes (CNTs) grafted w/poly(acrylic acid) (PAA)	Ag/MoO_x/spiro-OMeTAD /$MAPbI_3$/SnO_2/ITO/glass	21.2% (aver.) (18.6%)	80.9% after 800 h (30%) *Ambient air, 30% RH	2.9 ppm after immersion in water for 10 h (9.5 ppm)	–	[58]
	Poly(ethylene glycol)-b-poly(dimethyl siloxane)-poly(ethylene glycol)-chloride (PECL)	Au/Cr/BCP/PCBM + C60/$CsPbI_2Br$ + PECL/ NiO_x/ITO/glass	23.11% (best) 22.83% (aver.) (20.02%, 19.76%)	92% after 1008 h (85 °C, N_2, dark)	–	–	[59]
	Methyl 3-amino-2-thiophene-carboxylate (MATC)	Ag/BCP/C60/$(Cs_{0.17}FA_{0.83})$ $Pb(I_{0.9}Br_{0.1})_3$+MATC/PTAA/ITO/glass	21.51% (best) (19.67%)	90% after 800 h (80 °C, N_2) (control: 74.9%)	–	–	[60]
Additive (anti-solvent)	Zinc porphyrin (ZnP)	Ag/PCBM/$MAPbI_3$ /mesoporous TiO_2 (mp-TiO_2) /ZnO-MgO-EA^+/FTO/glass	19.26% (best) 20.53% (aver.) (18.21%, 19.77%)	77% after 900 h (27% after 500 h) *85 °C	N/A	–	[61]
	Poly(butyleneadipate-coterephthalate) (PBAT)	Au/Cr/BCP/OCBM + C60 /$Cs_{0.15}MA_{0.45}FA_{0.4}PbI_3$ (PBAT) /NiO_x/ITO/glass	22.07% (best) (19.17%)	90% after 3000 h (57%) *85% RH	10.70 ppm after immersion in water for 240 min (25.71 ppm)	–	[62]
	3-Mercaptopropyl-tri-ethoxy-silane (SiSH)	Ag/spiro-OMeTAD /$Rb_{0.02}(FA_{0.95}Cs_{0.05})_{0.98}PbI_{2.91}Br_{0.03}Cl_{0.06}$ (SiSH)/SnO_2/ITO/glass	22.42% (best) 22.21% (aver.) (20.80%, 20.67%)	95% after 500 h (60%) *dark, 25 °C, 40–45% RH	1.205 ppm after immersion in water for (3.551 ppm)	–	[63]
Bilayer (or buffer layer)	1H, 1H, 2H, 2H-perfluorode-canethiol (PFDT)	PFDT@Ag/BCP/PCBM/PFDT @$Cs_{0.05}(FA_{0.85}MA_{0.15})_{0.95}Pb(I_{0.85}Br_{0.15})_3$ /NiO/FTO/glass	21.79% (best) 20.65% (aver.) (20.15%, 19.03%)	90.1% after 500 h (46.2%) *N_2 atmosphere, 85 °C	2.05 ppm after immersion in water for 200 min (12.28 ppm)	–	[64]
	1,2-Ethanedithiol (1,2-EDT)	Ag/spiro-OMeTAD /1,2-EDT/$FA_{0.24}MA_{0.64}Cs_{0.12}PbI_{2.63}Cl_{0.37}$ /SnO_2/ITO/glass	21.0% (best) (19.16%)	>87% after 1005 h (66%) *Ambient air, RT, 40–60% RH	~17.5 ppm after immersion in water for 30 min (~25 ppm)	–	[65]
	Diphosphatidyl-glycerol (cardiolipin, Di-g)	PDMS/Ag/PCBM/BCP /Di-g/pero/PEDOT:PSS/PEN /hc-PEDOT/PDMS	20.29% (best) 19.41% (aver.) (18.80%, 17.70%)	85% after 10,000 bending cycles	Not detected after immersion in water for 48 h w/encapsulation (20 ppm)	15.01% *25 cm^2	[66]
	Photocurable benzyl acrylate (BzA)	Au/spiro-OMeTAD/BzA /$FA_{0.42}MA_{0.06}Cs_{0.52}PbI_{2.91}Br_{0.06}Cl_{0.03}$ /SnO_2/ITO/PET	20.86% (best) (19.07%)	80.1% after 400 h (30%) *Module (24 cm^2, active area), RT, 75% RH	*module 2.1 ppm after immersion in water for 240 min (12.3 ppm)	16.75% (14.79%) *24 cm^2	[67]
	2D π-conjugated benzodifuran-based polymer (PBDFP-Bz)	Au/spiro-OMeTAD /PBDFP-Bz/perovskite/SnO_2/ITO	21.73% (best) 20.52% (aver.) (19.55%, 19.21%)	92.2% after 720 h (64.4% after 720 h) *2.1×10^5 ppm O_2, 25–30 °C, ~30% RH	18.9 ppm after immersion in water for 7200 min (68.4 ppm)	–	[68]

(*continued on next page*)

Table 1 (*continued*)

Method	Passivation materials	PSC architectures	PCE (control PCE)	Stability (control stability) *Stability condition	Pb leakage (Pb leakage for control)	Module PCE (control) *Size	Ref.
	Poly-l-lysine w/sulfonic acid group (PLLS)	Au/spiro-OMeTAD /$(FAPbI_3)_{0.95}(MAPbBr_3)_{0.05}$/$TiO_2$ /FTO/glass	22.31% (best) (20.60%)	80% after 960 h (80% after 100 h) *RT, 10% RH	N/A	18.4% (16.4%) *36 cm^2	[69]
	2,2′,2″,2‴-(((9,9′-Spirobi [fluorene]-2,2′,7,7′ tetrayltetrakis(phe-nylazanediyl)) tetrakis(ethane-2,1-diyl))tetr-akis(oxy))tetrakis(-ethan-1-ol) (Spiro-OH) and 1,5-naph-thalene diisocyanate (NDI)	Ag/spiro-OMeTAD/spiro-NPU (in situ copolymerized layer) /$CH_3NH_3PbI_3$/SnO_2/FTO/glass	21.69% (best) 20.06% (aver.) (20.51%, 19.45%)	>90% after 500 h (42%) *Ambient air, 85 °C, 55% RH	<1 ppm after immersion in water for 20 d (~17 ppm after 1 h)	–	[70]
2D perovskite	1-Ethyl-3-methylimidazolium Bromide ionic liquid ([EMIM] Br) IL	Au/spiro-OMeTAD /ionic-liquid-perovskite capping layer /perovskite/SnO_2/FTO/glass	24.33% (best) (22.67%)	≈90% after 1000 h (≈80%) *RT, 30% RH	N/A	20.33% (18.8%) *10.75 cm^2	[71]
	1-Decyl-3-methylimidazolium bromide (DMIMB)	Au/spiro-OMeTAD /2D $[CsPbI_3]_{0.05}[(FAPbI_3)_{0.85}(MAPbBr_3)_{0.15}]_{0.95}$ (DMIMB) /$[CsPbI_3]_{0.05}[(FAPbI_3)_{0.85}(MAPbBr_3)_{0.15}]_{0.95}$/$TiO_2$/FTO/glass	22.40% (best) 21.23% (aver.) (21.17%, 19.77%)	67.7% after 660 min (27.6%) *50 °C, 50% RH	N/A	18.43% (17.02%) *25 cm^2	[72]
	ortho-(Phenylene) di(ethylammonium) iodide (*o*-$PDEAI_2$)	Au/spiro-OMeTAD /$FA_{0.81}MA_{0.24}Cs_{0.05}PbI_{2.77}Br_{0.04}Cl_{0.19}$ (*o*-$PDEAO_2$) /$FA_{0.81}MA_{0.24}Cs_{0.05}PbI_{2.77}Br_{0.04}Cl_{0.19}$ /TiO_2/SnO_2/FTO/glass	23.92% (best) 22.45% (aver.) (21.94%, 20.71%)	85% after 1008 h (58%) *Module (26 cm^2, active area), 40–50% RH	N/A	21.36% *26.00 cm^2	[73]
	n-Hexylamine (NHA)	Ag/spiro-OMeTAD /alkylated amorphous perovskitoid /$MAPbI_3$/SnO_2/ITO/glass	21.5% (best) 20.5% (aver.) (18.7%, 16.2%)	94% after 30 d (32%) *25 °C, ~55% RH	63.6 ppm placed in pH ~5.7 water for 60 s (120 ppm)	–	[74]
	(Z)-2-([1,1′-biphenyl]-4-yl)-3-(4-(3-aminopropoxy)phenyl) acrylonitrile (BPCSA)	Ag/BCP/$PC_{61}BM$/$FAPbI_3$/NiO_x/ITO/glass	23.45% (best) (19.07%)	90% after 4000 h (65 ± 5%, 25 °C) (control: 45%)	–	–	[75]

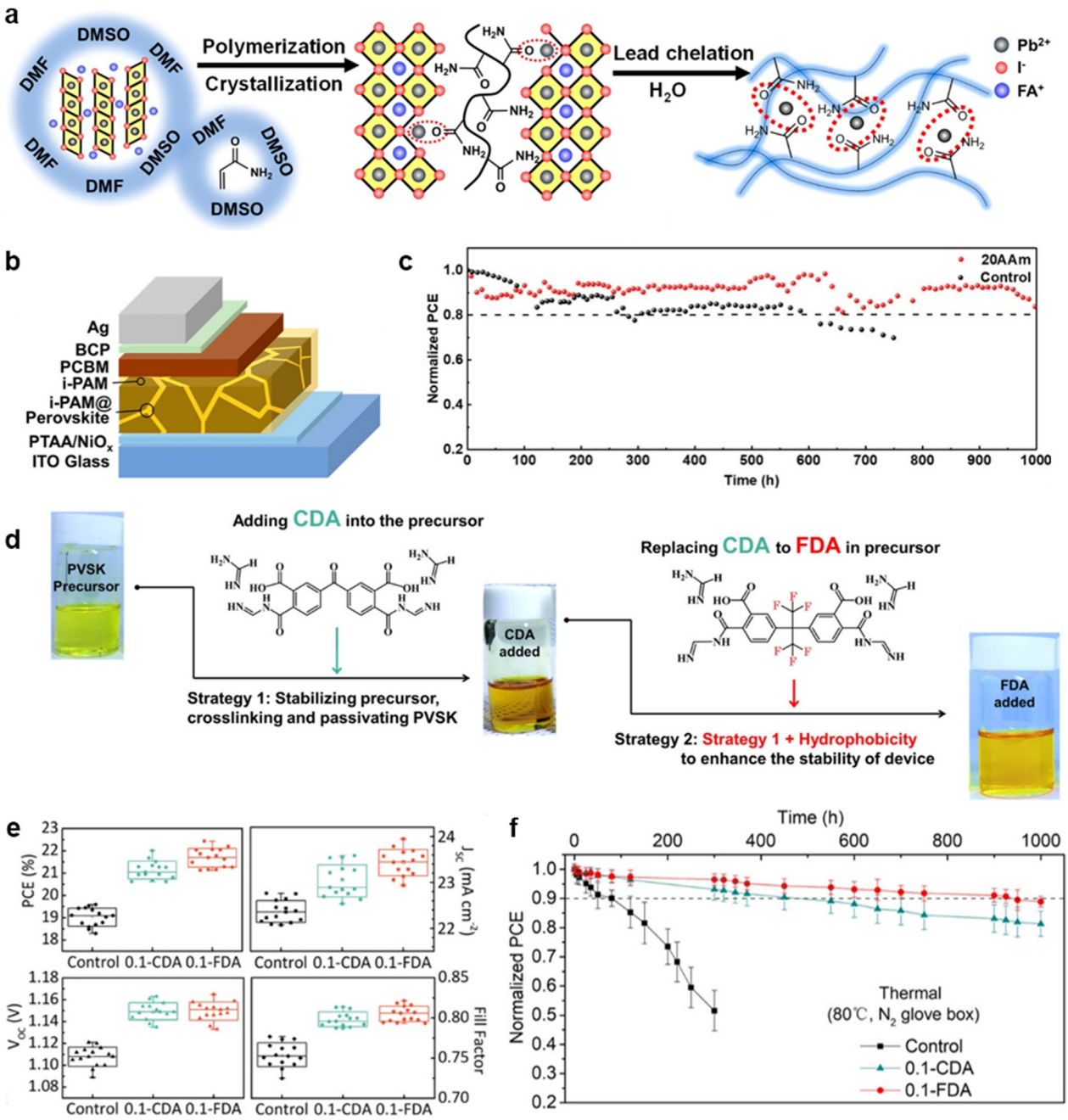

Fig. 3. Schematic illustration of (a) a Pb-leakage blocking strategy using polymerizable additives and (b) structure of inverted PSCs fabricated using an in situ polymerized network. (c) Normalized power output comparison between control PSCs and PSCs with 20 mg/mL AAM additive (20 AAm) at the maximum power point under one sun illumination. Reproduced from Ref. [53]. Copyright 2021 American Chemical Society. (d) Illustration of strategy for enhancing device stability by replacing CDA to FDA in precursor. (e) Statistics of photovoltaic parameters and (f) thermal stability of unencapsulated control, 0.1%-CDA, 0.1%-FDA devices. Reproduced from Ref. [56]. Copyright 2021 American Chemical Society.

carbonyl in the polymerized ZnP coordinated with the Pb ions on the perovskite surface, which effectively reduced the trap density and suppressed nonradiative recombination. Thus, the ZnP-incorporated PSCs exhibited a PCE of 20.53% with enhanced thermal stability, maintaining 77% of the initial efficiency even after 900 h of continuous heating at 85 °C. Another effective additive, the eco-friendly biodegradable plastic PBAT, has also been introduced to passivate various trap sites including Pb and neutral iodine. The carbonyl groups and benzene rings present in PBAT effectively passivated these trap sites, leading to significant improvements in the PCE and overall stability of the PSCs [62]. SiSH, which contains sulfhydryl (–SH) groups and siloxanes, was also employed as an additive to enhance the PSC stability [63]. SiSH offered advantages including Pb defect passivation through the sulfhydryl group and protection from moisture through the hydrophobicity of siloxanes. Furthermore, the flexible SiSH chain contributes to stress mitigation in perovskites. The SiSH-incorporated PSCs achieved a high PCE of 22.42% and high humidity stability.

Another approach to enhance the operational stability is to form a bilayer between the CTL and perovskite layer. Similar to the aforementioned studies using additives with functional groups, these bilayers include various functional groups to passivate the surface defects on the perovskite. The bilayer also acts as a protective wall against water/oxygen penetration and Pb leakage [64]. Wang *et al.* applied a coating of 1, 2-EDT with a thiol group on the perovskite layer to passivate surface

defects [65]. The thiol group strongly coordinated with the Pb ions, effectively passivating the defects and suppressing carrier recombination (Fig. 4a). Additionally, the hydrophobicity of the 1,2-EDT-coated perovskite improved the humidity resistance, presenting only 13% decay even after 1005 h exposure to 40–60% RH (Fig. 4b). The introduction of a two-dimensional (2D) π-conjugated benzodifuran-based polymer, PBDFP-Bz, comprising a benzodifuran backbone and multifunctional group between the perovskite and charge-transfer layers has been reported [68]. Such polymers have demonstrated superior charge mobility [78,79], and specifically, PBDFP-Bz exhibits a deep-lying molecular orbital energy level. This leads to beneficial charge transport and extraction optimization, resulting in improved PSC performance. Furthermore, the abundant functional molecules present in PBDFP-Bz, (C–N, C–S, and C–F) and their electron-rich characteristics effectively passivated surface defects. Additionally, the long alkyl side chain in PBDFP-Bz enhanced the moisture resistance, resulting in a high PCE of 21.73% and excellent stability (92.2% of initial PCE after 720 h under ambient conditions). Di-g, comprising hydrophilic phosphonic acid groups and a hydrophobic end, was employed in flexible PSCs [66]. The embedded Di-g layer simultaneously interacts with phosphonic groups and prevents water penetration, thereby enhancing the long-term stability. In flexible PSCs, this layer also provides mechanical stability during device operation by releasing residual stress in the perovskite surface region, thereby decreasing damage during the bending cycles (85% of initial PCE after 10,000 bending cycles). Similarly, Zhu *et al.* employed BzA as an interfacial layer in flexible PSCs [67].The carboxyl (C=O) group in BzA directly coordinated with Pb ions, effectively suppressing the trap density, and preventing water, oxygen, and Pb leakage. Consequently, the optimized PSCs exhibited remarkable long-term stability against moisture, retaining 81.0% of their initial PCE, even after 400 h at 75% humidity. Guo *et al.* reported a bilayer that not only passivated surface defects in perovskite, but also addressed undercoordinated defects in the ETL [69]. They introduced the non-toxic eco-friendly PLL between the TiO_2 and perovskite layers after modifying PLL with a sulfonic acid group without changing the bandgap energy (Figs. 4c and d). The PLLS sulfonic groups effectively passivate oxygen vacancies and defects in TiO_2 by reacting with under-coordinated Ti ions, whereas the amine groups effectively passivate deep-level surface defects on the perovskite. The implementation of PLLS in PSMs has led to remarkable stability achievements, surpassing expectations not only for PSCs but also for the entire module (Fig. 4e). Additionally, the introduction of a modified HTM can enhance photovoltaic performance and stability [70]. Spiro-NPU, synthesized by the copolymerization of Spiro-OH and NDI monomers, exhibited a well-matched energetic structure with the perovskite layer, facilitating effective hole transfer while preventing electron back-transfer. Consequently, the PSCs incorporating the spiro-NPU bilayer demonstrated remarkable stability, maintaining nearly 100% of their initial PCE, even after 3000 h at 60% RH and 25 °C in air. Despite the significant progress achieved through the incorporation of additives and interfacial bilayers, it is crucial to carefully design the characteristics of these additives and bilayers to ensure that they effectively fulfill their intended functions without compromising charge transportation within the device.

The formation of an additional 2D perovskite layer on the perovskite surface is another good passivation strategy. Zhu *et al.* used an IL to passivate defects by forming a thin IL-state perovskite layer on a 3D perovskite surface [71]. The IL [EMIM]Br was employed for $HC(NH_2)_2PbI_3$ ($FAPbI_3$) PSCs, which anchored the Pb^{2+} and I^- ions via strong ionic bonds thereby enhancing the stability and efficiency. Another IL—DMIMB—enhanced the stability by forming a 2D perovskite layer [72]. These layers retard the charge recombination by passivating defects and improve the charge extraction through their suitable band-energy alignment. Typically, 2D perovskite layers are formed via organic halide salt treatment; this leads to an in-plane formation preference that results in compromised charge transport and hindered photovoltaic performance during working hours, particularly under

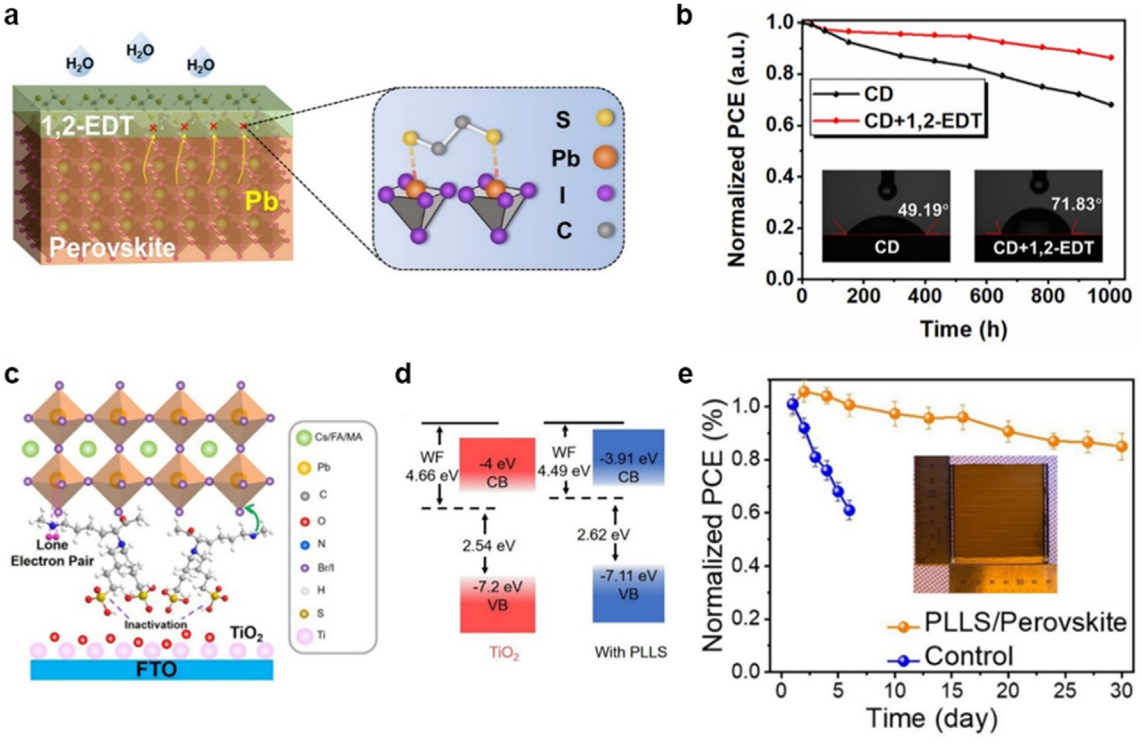

Fig. 4. (a) Schematic of 1,2-EDT-treated perovskite layer and its coordination with Pb. (b) Long-term stability of a PSC fabricated with/without 1,2-EDT treatment under 40–60% RH at ambient atmosphere. Inset: contact angles of perovskite layers with/without 1,2-EDT. Reproduced from Ref. [65]. Copyright 2022 Wiley-VCH. (c) Schematic of interlayer PLLS and its function and (d) energy level diagram of TiO_2 layer with/without PLLS modification. (e) Long-term stability of PSMs fabricated with/without spiro-NPU under ambient air (RT, 5–10% RH). Inset: optical image of a 6 × 6 cm^2 PSM. Reproduced from Ref. [69]. Copyright 2023 Elsevier.

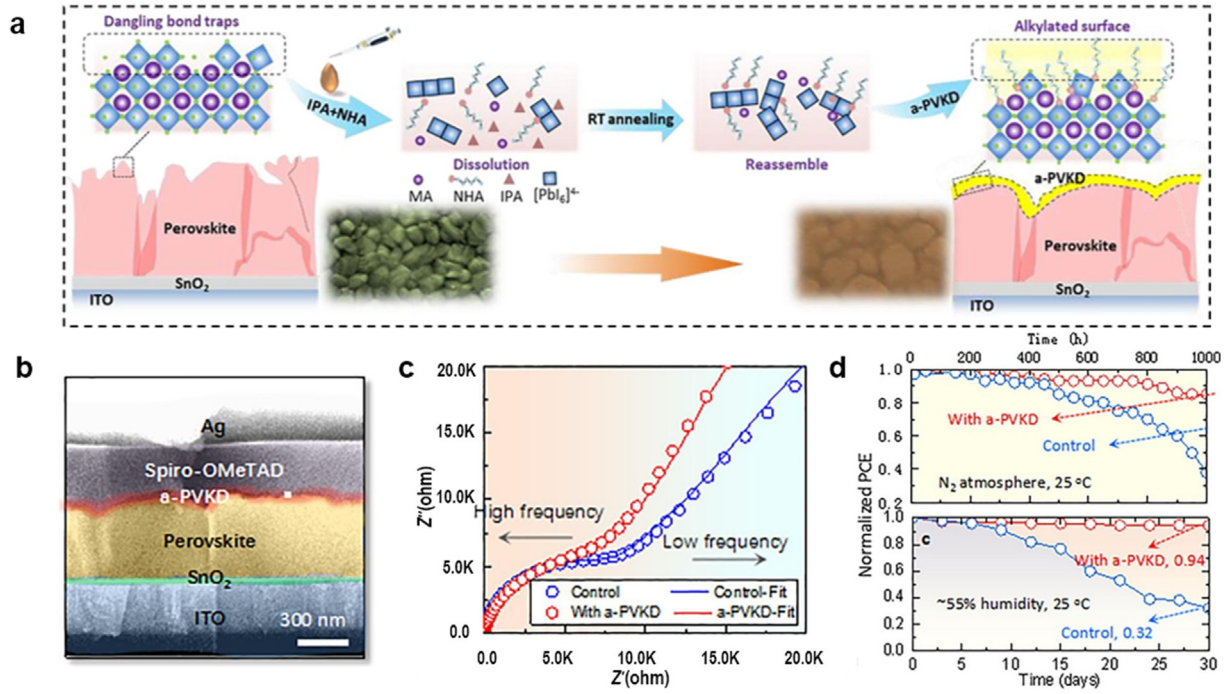

Fig. 5. (a) Schematic diagram of the a-PVKD formation process and (b) cross-sectional image of an a-PVKD-assembled PSC. Comparison of the (c) Nyquist plots and (d) stability under specific conditions of the control PSC and PSC fabricated with a-PVKD. Reproduced from Ref. [74]. Copyright 2022 Elsevier.

high-temperature conditions [80,81]. To address these issues, Liu *et al.* investigated various 2D perovskite structures by incorporating *ortho*-, *meta*-, and *para*-$PDEAI_2$ [73]. Among them, *o*-$PDEAI_2$ afforded an increased energy barrier, preventing the formation of in-plane 2D perovskite and inhibiting organic cation migration into the perovskite lattice, even at high temperatures. Consequently, PSCs passivated with *o*-$PDEAI_2$ achieved a high PCE of 23.9% and demonstrated enhanced long-term stability for over 1000 h. Recently, an a-PVKD/c-PVK heterostructure was employed by reconstructing c-PVSK using a post-treatment solution (Fig. 5) [74]. Both devices (PSCs with/without the a-PVKD interlayer) exhibited similar series resistances (R_s), indicating that the a-PVKD interlayer did not impede charge transport. However, the control device had a significantly lower recombination resistance (R_{rec} = 17,225 Ω) than the a-PVKD-based device (23,137 Ω), indicating that this layer effectively suppressed recombination within the device (Fig. 5c). Moreover, the a-PVKD layer effectively terminated defects on the perovskite surface, acting as a moisture barrier and passivating defects on the c-PVK surface, thereby resulting in enhanced operating stability (> 85% of initial PCE after 1000 h; Fig. 5d).

Additionally, temperature variations induce residual strain owing to the higher thermal expansion coefficient than that of the other layers, resulting in PSC degradation over time. The internal stresses generated during the formation of perovskite films are usually substantial, impacting device performance negatively and contributing to degradation. Several strategies have been employed to alleviate internal stress in the perovskite layer. One common approach involves reducing internal stresses by lowering the annealing temperature of the perovskite layer. Rolston *et al.* reported a reduction in residual stresses by eliminating the annealing process [82]. Additionally, tensile stress can be significantly decreased by minimizing the thermal coefficient mismatch. Given the high coefficients of thermal expansion (CTE) in perovskites, the use of high CTE polymeric substrates can reduce tensile stress and enhance PSC stability [82]. In addition, introducing a buffer layer or CTL with high CTEs can effectively relax internal stress, further improving PSC stability. Alkyltrimethoxysilanes have been employed between the TiO_2 and perovskite ($CsPbI_3$) layer as a strain-released layer, with the longest alkyl chain proving most effective in suppressing lattice distortion and enhancing stability (retaining 80% of initial PCE after 3228 ± 91 h under 40 °C one sun illumination test for encapsulated PSCs) [83]. Another strategy to reduce internal stress involves modulating lattice distortion. Huang *et al.* mitigated interfacial lattice distortion by passivating the TiO_2 surface with gaseous fluorine [84]. Additionally, the introduction of 2D WS_2 nanoflakes helped relax internal strain, demonstrating remarkable stability over 120 days under 80% humidity at 25 °C [85]. Recently, light-induced cross-linking of acrylamide (Am) monomers was employed to enhance the efficiency and stability of PSCs [86]. The Am monomers promote the preferred crystal orientation of perovskite, and their liquid properties effectively alleviate lattice strain during the crystallization of perovskite film. Consequently, PSCs treated with Am exhibited high moisture stability (retaining 80% of initial PCE after 700 h under ≈ 55 ± 5% RH) and light stability (retaining 80% of initial PCE after 1008 h under one sun illumination). It is crucial to note that controlling internal stress can enhance PSC stability, representing a potentially intriguing area for further exploration. However, attributing stability issues solely to internal stress proves challenging; thus, comprehensive research should consider various factors influencing stability.

Intrinsic stability challenges further complicate the development of Perovskite solar modules (PSMs). Passivation emerges as an efficient way to enhance stability and PCE, even for large-area PSMs. Zhu *et al.* achieved a notable PCE of 18.27% from PSMs with an active area of 60.68 cm^2 [23]. The PSMs retained 80% of their initial PCE after 1800 h under ~45 °C and one sun illumination, showcasing the potential adoption of additives for commercial viability. PSMs, featuring interconnected subcells, manifest heightened contact and series resistance, resulting in accelerated degradation due to increased joule heat as the active area expands. Additionally, exposed perovskite interfaces and direct contact interfaces between metal electrodes and perovskite expedite the degradation process. The P2 and P3 scribe processes present additional challenges by elevating the defect density at the perovskite interfaces. In view of these combined factors, to effectively address the intricate challenges associated with achieving intrinsic stability in PSMs, meticulous and comprehensive studies are required.

3.1.3. Encapsulation

PSCs are vulnerable to degradation when exposed to environmental stimuli, including moisture, heat, oxygen, and UV radiation, owing to the poor chemical stability of the perovskite layer. To enhance the extrinsic stability of PSCs, encapsulation approaches have been employed to isolate devices from these external factors. PSC encapsulation techniques were initially performed using polymers and glass coverslips [87,88]. However, the most recommended method for encapsulating PSCs is glass–glass encapsulation, which can be performed with/without additional epoxy/polymeric encapsulation materials and different edge sealants [89]. Shi *et al.* demonstrated a cost-effective encapsulation strategy using glass with PO/PIB-based polymeric sealants [6]. These polymers serve as effective moisture barriers and strong adhesives between the cover glasses and PSCs, resulting in enhanced stability. The PIB-encapsulated PSCs exhibited excellent performance retention even after 1800 h of damp heat testing, surpassing the IEC 61215:2016 standard (1000 h). Polymer layers offer an alternative encapsulation strategy that is applicable to both rigid and flexible PSCs, making them versatile options for various device configurations. These strategies include liquid, film, and evaporation forms, depending on convenience and specific requirements. However, such polymers often have free volumes or pinholes within their films, which limit their effectiveness as barriers [90]. To overcome this, multilayer encapsulation techniques have been demonstrated to improve stability [24,91–93]. However, although multilayers enhance stability, they may lead to reduced transmittance and thereby necessitate a trade-off between stability and photovoltaic efficiency.

The stability of PSCs can be enhanced, without compromising their photovoltaic efficiencies, by applying AR coatings in the encapsulation [94–97]. Cho *et al.* employed a PPFC thin film on flexible PSCs to enhance their PCE [96]. The PPFC thin film significantly increased the PCE from 18.6% to 20.4% by improving light transmittance through its antireflection effect, which was attributed to its low refractive index of 1.38. Additionally, the hydrophobic nature of the PPFC film protected the PSCs from moisture and removed contaminants from the surface, resulting in high long-term stability with a retention rate of 80.6 ± 6.0% of the initial PCE after 957 h of testing at 25 °C and 65% RH.

Furthermore, encapsulation techniques not only improve the PSC stability but also address environmental concerns by effectively blocking the toxic Pb leakage (Table 2). Various Pb-adsorbing materials have been employed in encapsulation strategies to effectively prevent Pb leakage [98,99,101–104]. Inogel-based encapsulation using polyacrylic acid has been developed to enhance stability and reduce Pb leakage, achieving effective Pb leakage reduction > 99% under simulated hail and car rolling tests [102]. Li *et al.* employed S-GA combined with PDMS as an encapsulant for flexible PSCs, demonstrating both bendability (≈84% of initial PCE after 3000 cycles bending test) and long-term stability (~90% of initial PCE after 500 h under 40–50% RH at 25 °C) (Fig. 6) [104]. Additionally, the encapsulant exhibited a high maximum Pb adsorption capacity of 520.83 mg/g, resulting in > 99% reduction in Pb leakage (< 10 ppb) in various real-world simulated tests that included acid rain, bending, and thermal circling. Detailed information regarding the encapsulation strategies is provided in Table 2. These advancements in enhancing the stability and reducing the environmental impacts can greatly contribute to the accelerated commercialization of PSCs.

3.2. In situ regeneration

As mentioned previously, extensive research has been conducted to enhance the PSC stability using passivation and encapsulation approaches. However, the long-term stability and overall lifetime of PSCs have not yet reached the desired levels for commercialization. To address this, recent efforts have focused on the in situ regeneration of PSCs using two primary approaches: self-healing and reuse. These approaches aim to restore the initial PSC performance following damages caused by environmental stresses, including light, thermal, and mechanical factors, to extend the overall lifetime.

3.2.1. Self-healing

PSC self-healing is an effective strategy to enhance their stability, which can restore them to their original state (Table 3). There are several reports on the reversible decomposition–reconstruction of perovskite under dark conditions [105–109]. Light-induced damage to perovskite results in phase segregation or metastable trap states that can be restored through a certain relaxation time in the dark [107,109]. Such self-healing behaviors involve defects or ion migration; thus, the recovery rate could be affected by the perovskite composition [105], defects [106], and temperature [107]. Ceratti *et al.* investigated the influence of the perovskite composition on the self-healing performance [105]. Among the single perovskite crystals with an $APbBr_3$ structure, $FAPbBr_3$ demonstrated the fastest self-healing ability, whereas $CsPbBr_3$ exhibited a slower recovery. This behavior was attributed to the lower Cs and Br activities, which make $CsBr_3$ formation harder than those of $MABr_3$ and $FABr_3$. Moreover, the slow recovery rate was attributed to energy barriers that hinder detrapping of ion defects from grain boundaries. The recovery process initiates at the grain boundary and progresses towards the grain center in Ref. [106]. Additionally, photoinduced degradation can be fully reversed by thermal activation in the absence of light, and the recovery rate tends to increase at higher temperatures [107].

To ensure a long-lasting self-healing performance, it is crucial to prevent the decomposed perovskite species, including halides and cations, from escaping. Halogen ions, especially I^- ions, have a high diffusion coefficient (~10^{-12} cm^2/s) [120], which causes continuous migration toward the electrode. Consequently, the diffused I^- ions react with diffused Ag^+ ions to form stable AgI composites. This gradual perovskite decomposition hinders full recovery, primarily because of the loss of I^- ions. Consequently, the Ag electrode was replaced with an ITO electrode to prevent the formation of AgI composites (Fig. 7a) [108]. The ITO electrode inhibited the decomposed I^- ions from migrating, leading to saturation at the perovskite/ITO surface without I^- consumption under light conditions. Subsequently, the saturated I^- ions recovered the corresponding vacancies under dark conditions, displaying 90% of the initial PCE even after 17 harvesting–rest–recovery cycles (Fig. 7b). Owing to the volatile characteristics of perovskite, several gaseous byproducts from its thermal degradation [121,122], can also significantly impact the self-healing performance by causing a loss in the perovskite composition. Therefore, efforts have been made to prevent decomposed volatile species from escaping from perovskite. Zhao *et al.* introduced a polymer-scaffold PSC that demonstrated an impressive *J*–*V* curve recovery to its original state within 45 s (Fig. 7c) [111]. The use of the highly hygroscopic PEG as a polymer-scaffold material allowed for the formation of a compact barrier to prevent moisture penetration. Additionally, PEG was anchored around the perovskite layer, interacting with MAI and preventing it from escaping. After preventing the loss of MAI, the PbI_2 within the perovskite layer reacted with the retained MAI to regenerate the perovskite in a process similar to the two-step perovskite synthesis. A similar study reported self-healing PSCs using PVP, which acted as an anchor for MAI through hydrogen bonding between the PVP C=O and MA N–H groups [112]. The PVP-containing perovskite film showed rapid recovery within 30 s after being exposed to water spraying for 60 s. Notably, the PVP-incorporated PSCs exhibited repeatable self-healing properties, retaining 50% of their initial PCE after three cycles of self-healing tests involving 60 s of exposure to water. Borate salt (borax) combined with PMMA was also employed to enhance the self-healing properties (Fig. 7d) [110]. The addition of borax resulted in the formation of a dense barrier, promoting enhanced self-healing properties. The degraded PSCs subjected to 10 h of one sun illumination exhibited remarkable recovery, with over 95% of their initial PCE after two cycles of working/self-healing processes involving 12 h resting under dark conditions (Fig. 7e). Encapsulation is another effective strategy to prevent decomposed perovskite species from escaping from PSCs. Lv *et al.* developed a bilayer encapsulation approach by applying the sequential deposition of compact Al_2O_3 and hydrophobic 1*H*,1*H*,2*H*,2*H*-perfluorodecyltrichlorosilane layers, preventing volatile organics

Table 2
Summary of various strategies for stability enhancement by encapsulation.

Encapsulation materials	PSC architectures	PCE (control PCE)	Stability (control stability) *stability condition	Pb leakage (Pb leakage for control)	Module PCE (control) *size	Ref.
Glass with polyisobutylene (PIB)-based sealant	Glass/PIB/Au/PTAA /$Cs_{0.05}FA_{0.8}MA_{0.15}Pb(I_{0.85}Br_{0.15})_3$/mp-$TiO_2$ /compact TiO_2 (c-TiO_2)/FTO/glass	13.8% (best) 13.3% (aver) (14.1%, 13.5%)	Survival after 1800 h *85 °C, 85% RH Survival after 75 cycles *40–85 °C	–	–	[6]
Parylene/MgF_2/Al_2O_3	Al_2O_3/MgF_2/parylene/Ag/BCP/PCBM /$FA_{0.85}Cs_{0.15}Pb(Br_{0.15}I_{2.85})$/NiMgLiO /FTO/glass	19.86% (19.85%)	96% after 100 h *85 °C, 85% RH	–	–	[91]
Perhydropolysilazane (PHPS)/ poly(ethylene terephthalate) (PET)/PHPS	PHPS/PET/PHPS/Au/spiro-OMeTAD /$MAPbI_3$/SnO_2/FTO/glass	17.36% (17.37%)	90% after 1000 h *ambient air	–	–	[92]
Glass with polyvinylpyrrolidone (PVP) and epoxy	Glass/epoxy/PVP/Ag /bathophenanthroline (Bphen) /[6,6]-phenyl-C61-butyric acid methyl ester ($PC_{60}BM$)/$MAPbI_3$ /poly-TPD(2,3,5,6-tetrafluoro-7,7,8,8-tetracyanoquinodimethane(F4-TCNQ) /ITO/glass	15.26% (15.62%)	80% after 1000 h *AM 1.5 irradiation	–	–	[24]
Glass/CeO_2/SiO_2/TiO_2/PDMS	Carbon/$MAPbI_3$/TiO_2/FTO/glass/CeO_2 /SiO_2/TiO_2/PDMS	16.60% (14.92%)	98.5% after 31 d *50 °C, 90% RH, w/UV lamp	–	–	[95]
Plasmapolymerized-fluorocarbon (PPFC)	Au/spiro-OMeTAD /$(FAPbI_3)_{0.95}(MAPbBr_3)_{0.05}$/$SnO_2$/ITO /PET/PPFC	20.4% (18.6%)	97.7% after 100 h *25 °C, 65% RH	–	–	[96]
Glass with acrylate hot melt adhesive (AHMA) and polyvinyl butyral (PVB)	Glass/PVB/AHMA/Au/MoO_3 /spiro-OMeTAD/2-Phenylethylamine hydroiodide (PEAI) /$CsFAMAPbI_3$/SnO_2/ITO/glass	20.88% (21.58%)	–	703 ppb after dripping water for 6 h (control: 17.32 ppm)	–	[97]
Glass or plastic sheet with sulfonic acid cation exchange resins (Pb-adsorbing resin)	plastic sheet/epoxy /Pb-adsorbing resin /Cu/BCP/C_{60}/$MAPbI_3$/PTAA/ITO/glass	20.6% (best) 20.1% (aver.) (19.8%, 19.3%)	~80% after 500 h *ambient air, 45 °C	11.9 ppb after exposure to dripping water for 1 h (control (w/o Pb-adsorbing resin): 16 ppm)	–	[98]
P,P′-didi-phosphonic acid (DMDP), ethylene vinyl acetate (EVA) w/n,n,n',n',-ethylene-diamine-tetra-kis (methylene-phosphonic acid)-poly(ethylene oxide) (EDTMP-PEO)	EVA/EDTMP-PEO/Au/spiro-OMeTAD /$(CsPbI_3)_{0.05}(FAPbI_3)_{0.85}(MAPbBr_3)_{0.15}$ /TiO_2/FTO/glass/DMDP	20.12% (best) (19.69%)	Above 80% after 500 h *ambient air, 50 °C	Pb SQE[a] = 97.7% (at R.T.)	–	[99]
Glass w/epoxy resin-based polymers (diglycidyl ether bisphenol A, *n*-octylamine, *m*-xylylenediamine)	Glass/Au/spiro-OMeTAD /$Cs_{0.07}FA_{0.93}PbI_3$/c-TiO_2/FTO/glass	N/A	N/A	< 1.8 mg/h m^2 after dripping acid water (pH = 4.2) on damaged PSM for 1.5 h (control: 34 mg/h m^2)	14.3% (14.1%) *12.0 cm^2	[100]
Glass w/3-mercaptopropyl) trimethoxysilane-capped nanospheres (MPTMS-ns)	Glass/Si adhesive + MPTMS-ns/Au /spiro-OMeTAD /$Cs_{0.05}(MA_{0.17}FA_{0.83})_{0.95}Pb(I_{0.83}Br_{0.17})_3$/$SnO_2$ /FTO/glass	~7% (no significant difference between encapsulated and control devices)	N/A	Pb SQE = 98%	–	[101]
Glass w/poly acrylic acid (PAA) inogel	Glass/inogel/polyolefin(POE)/Cu /bathocuproine(BCP)/C_{60}/$MA_{0.7}Fa_{0.3}PbI_3$ /poly(bis(4-phenyl) (2,4,6-trimethylphenyl) amine) (PTAA) /ITO/glass/inogel /polydimethylsiloxane (PDMS)	22.9% (best) 21.7% (aver.) (22.45%, 20.9%)	95.2% after 1000 h *85 °C, 85% RH	0.63 ppb after immersed in water for 24 h (control: 10.65 ppm)	18.5% (17.2%) *31.5 cm^2	[102]
cation-exchange resins (CERs)		19.2% (best) (19.5%)	N/A	1.96 ppm after water dripping for 1 h (control: 13.24 ppm)	–	[103]

(*continued on next page*)

Table 2 (*continued*)

Encapsulation materials	PSC architectures	PCE (control PCE)	Stability (control stability) *stability condition	Pb leakage (Pb leakage for control)	Module PCE (control) *size	Ref.
	CER/carbon/SnO_2/C_{60} /$Rb_{0.05}Cs_{0.05}FA_{0.85}MA_{0.05}PbI_{2.85}Br_{0.15}$ /PTAA/ITO/glass					
Sulfonated graphene aerogels (S-GA) w/PDMS	PDMS-SGA/Ag/BCP/C_{60} /perovskite/PTAA/ITO/PEN/PDMS-SGA	22.68% (best) (22.60%)	> 90% after 500 h (< 20% after 350 h) *ambient air, 25 °C, ~40–50% RH	10.2 ppb after immersed in acid water (pH = 4.2) at 85 °C for 3 h (control: 214.72 ppm)	14.980% (14.857%) *25 cm^2	[104]

[a] SQE (sequestration efficiency, %) $= \left(1 - \frac{\text{Pb leakage from devices with encapsulation}}{\text{Pb leakage from devices without any encapsulation}}\right) \times 100\%$.

from escaping the decomposed PSCs [113]. The encapsulated PSCs exhibited reversible decay–recovery performance and demonstrated only slight decay under harsh conditions (85 °C, 85% RH) due to enhanced water resistance. These results indicate the feasibility of using well-encapsulated PSCs with reproducible self-healing properties.

Another PSC self-healing strategy involves Pb^0 and I^0 defect removal from the perovskite. Even in well-encapsulated PSCs, the Pb^+ and I^- ions undergo reduction/oxidation under external stimuli, leading to the formation of Pb^0 and I^0 defects and the subsequent decay in photovoltaic performance [123,124]. Wang *et al.* introduced a Eu^{3+}–Eu^{2+} ion pair as a "redox shuttle" to regenerate the perovskite by eliminating Pb^0 and I^0 defects. Eu^{3+} and Eu^{2+} ions cyclically oxidize Pb^0 and reduce I^0 defects, respectively [115]. Although the redox reactions of Y^{3+} and Fe^{3+} ions with Pb and I were also evaluated, the effectiveness of Y^{3+} ions was low, and the Fe^{3+} ions were too strong to oxidize I^-. Therefore, the utilization of Eu^{3+} ions as a "redox shuttle" for the regeneration of perovskite is a promising strategy. Chang *et al.* employed Fc as a recovery agent to eliminate I^0 and Pb^0 defects. The sandwich architecture of Fc with a Fe^{2+} core protects the perovskite layer by preventing its direct replacement by Fe^{2+} ions [114]. Fig. 7f shows the self-healing process through redox reactions, where the Fc/Fc^+ pair facilitates $FcPbI_3$ formation, effectively eliminating I^0 and Pb^0 defects. This is followed by the cyclical regeneration of perovskite and Fc, leading to the elimination of A-site elemental defects. Notably, after soaking in an Fc solution, the PCE of the degraded PSCs (14.9%) recovered to 16.0%, which is comparable to that (16.9%) of the original PSC (Figs. 7g and h). These results suggest the effectiveness of Fc for both self-healing and recovery of the degraded PSCs.

The flexibility of PSCs makes them highly suitable for use in wearable/foldable devices. However, flexible PSCs are prone to perovskite crystal brittleness when subjected to long-term bending/stretching, leading to a reduced photovoltaic performance and lifetime. Consequently, self-healing polymers have been used to enable PSCs to self-heal under external mechanical stresses. For example, self-healing SHP has been incorporated into perovskite films to repair cracks at the grain boundaries (Fig. 8a) [116]. SHP releases the external mechanical stress and repairs the cracks via extensive hydrogen bonding. The SHP-containing PSCs exhibited 80% recovery of their initial PCE after 800 cycles of 20% stretching testing (Fig. 8b), indicating the promising potential of self-healing polymers as a strategy for enhancing the durability and applicability of PSCs in wearable devices. Lan *et al.* proposed a thermally driven self-healing approach for flexible PSCs by incorporating PUDS, which comprises both hard and soft phases that provide high tensile strength and enhance resistance to bending [117]. When broken due to external mechanical stresses, the disulfide bonds in the hard phase recombine at response temperatures above 80 °C, enabling self-healing of the flexible PSCs after cracking (Figs. 8c–e). Through thermal annealing at 80 °C for 10 min, the PCE of the PUDS-incorporated flexible PSCs recovered to 15.12%, following a significant decrease in PCE from 17.19% to 2.06% after the bending test (Figs. 8f and g). Similarly, polyurethane [118] and thiourea-triethylene glycol polymer TUEG3 [119] have been utilized as self-healing polymers to address mechanical stresses in flexible PSCs, resulting in remarkable PCE recovery with the restoration of cracked device surfaces. These studies underscore the effectiveness of self-healing polymer approaches for achieving substantial PCE recovery, making them highly valuable for wearable and foldable devices. However, it is crucial to consider the requirement of adequate heat to restore self-healing polymers to their initial state. Therefore, the feasibility of their self-healing performance during operating life should be considered, necessitating further investigation.

3.2.2. PSC rejuvenation

The ability to prolong the limited lifetime of PSCs through regeneration would greatly benefit their sustainable and viable commercialization (Table 4). Huang *et al.* first reported the rejuvenation of degraded PSCs, leading to an extended lifetime exceeding 100 d [125]. At over 60 d of aging, the PSCs exhibited degradation in the vertical direction,

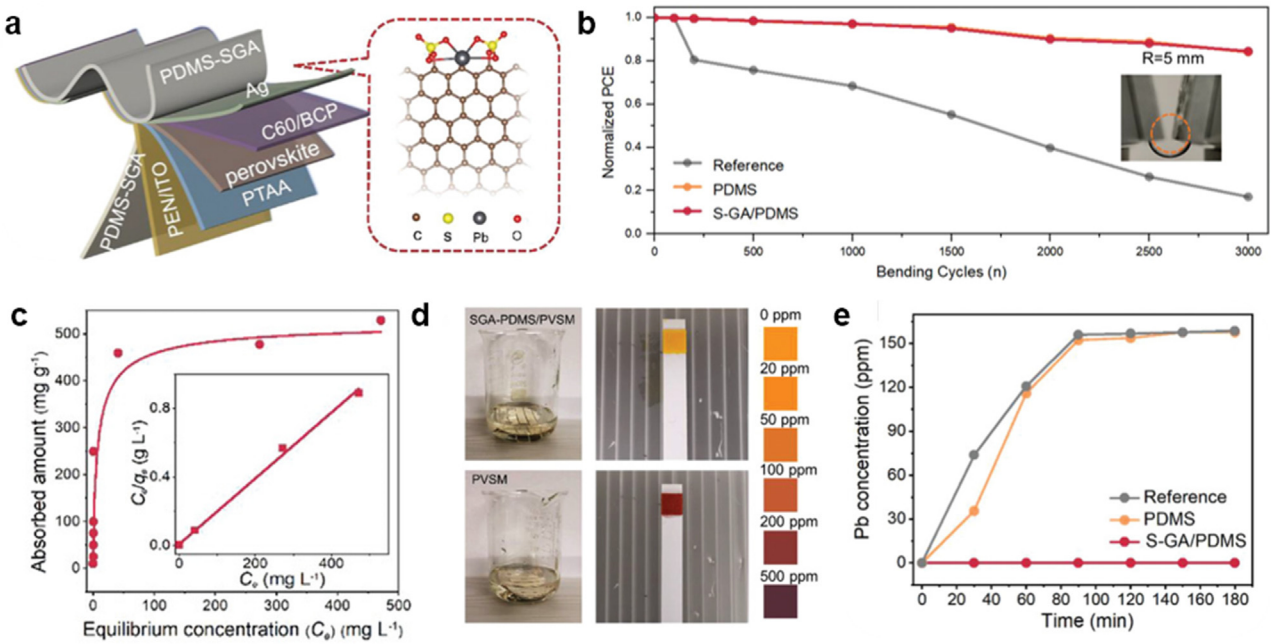

Fig. 6. (a) Schematic of flexible PSC encapsulated with S-GA/PDMS and computed minimum-energy adsorption model structures of Pb^{2+}. (b) Bendability of PSMs without/with different encapsulants under ambient conditions (40–50% RH, 25 °C, bending radius: 5 mm) and (c) Langmuir isotherms of S-GA for Pb^{2+} sorption. (d) Pb leakage test for degraded PSMs without/with S-GA/PDMS encapsulant and (e) Pb concentration of contaminated water containing PSMs without/with different encapsulants. Reproduced from Ref. [104]. Copyright 2021 Wiley-VCH.

resulting in two distinct areas: a degraded PbI_2 region (yellow) and a perovskite (black) region protected by gold electrodes. To address the horizontal degradation, the degraded PSCs were immersed in an MAI solution at 70 °C, which easily rejuvenated the PSC and achieved a PCE of 11.0%, comparable to that of the original PSC (11.6%), even after two aging–rejuvenation cycles. The spin coating of an MAI solution on a degraded $MAPbI_3$ perovskite layer also resulted in the regeneration of decayed photovoltaic performance [126]. This regeneration was attributed to the recrystallization of the $MAPbI_3$ structure after thermal annealing, which resembled the two-step perovskite synthesis process. To enhance the photovoltaic performance of the recovered PSCs, a sequential process to recover the degraded PSCs was introduced which involved the thermal decomposition of $MAPbI_3$ [127]. This process included removing the Ag electrode using adhesive tape and HTM using chlorobenzene. Subsequently, the perovskite layer was thermally annealed to decompose into highly crystalline PbI_2 with a mesoporous scaffold. This scaffold showed effective recovery of the degraded PSCs, exhibiting a PCE of 14.84% comparable to that of the original PSCs (14.35%). However, the PSC performance after the second recovery was reduced to 8.51%, possibly because of the excess remaining PbI_2. Chhillar *et al.* compared degraded perovskite films deposited using three different methods: single-step acetate, single-step chloride, and sequential deposition, as shown in Figs. 9a and b [130]. Among them, single-step acetate deposition resulted in an increase in PL intensity and a slightly blue-shifted peak after recycling, indicating improved film quality (Fig. 9c). Furthermore, the degraded perovskite films deposited via this route showed easy reconversion to the perovskite upon the introduction of MAI, attributed to the lower PbI_2 crystallinity compared to that of fresh PbI_2 (Fig. 9d). These findings highlight the importance of the characteristics of the degraded perovskite layer and the synthesis conditions of the perovskite film for the effective reuse of degraded PSCs. An unusual solid–liquid–solid phase transition induced by methylamine gas was also utilized to regenerate degraded PSCs [129]. The encapsulated $MAPbI_3$ PSCs achieved a remarkable recovery, with the PCE reaching 91% of its initial value after two degradation–regeneration cycles by introducing methylamine gas, despite the PSCs degraded to ~40% (Figs. 9c and d)). This approach enables on-site PSC regeneration without the need to replace any components, indicating its potential in terms of eco-friendliness and cost-effectiveness in PSC technology. The aforementioned regeneration studies demonstrate the potential of regeneration techniques to significantly prolong the lifetime of PSCs and enhance their commercial viability.

4. Post-end-of-life

Management of solar cells post their end-of-life poses critical issues for the future of energy resources. With the implementation of the 2012 revision of the WEEE Directive, the solar PV panels intended for disposal were categorized as WEEE within the European Union according to the WEEE Directive [131]. Consequently, producers were made responsible for the collection, recycling, and recovery of PV panels. In particular, PSCs contain noble metals and toxic materials that can cause significant environmental and economic issues. Therefore, the management of PSCs post their end-of-life is inevitable. In a recent study, Tian *et al.* investigated the landfill and recycling scenarios after the end-of-life stage for six types of PSCs [8]. The results showed that recycling strategies could significantly decrease the energy payback time by up to 72.6% and reduce the greenhouse gas emission factor by 71.2%. Consequently, recycling PSCs post their end-of-life has become a pressing concern that has led to several studies on the recycling of noble and toxic materials.

4.1. Noble material recycling

The LCOE of PSCs (~14 US cents/kW/h) is higher than those of other traditional PV technologies including Si, CdTe, and CiGS (5–10 US cents/kW/h, assuming a five-year lifetime). Although the LCOE significantly depends on the lifetime, reducing the fabrication cost remains important for commercialization. Recent research has estimated the cost of PSCs, revealing that the fabrication of FTO accounts for the highest portion (43%) of the total PSC cost [132]. Moreover, because TCO substrates include rare metals (e.g., In and Sn), efficient recycling is required. The metal electrode, particularly Au, also represents a substantial portion (18%) of the total cost [132,133]. Although substituting Au with cheaper alternatives (e.g., Cu, Ni, and Cr) reduces the cost of the metal electrode,

Table 3
Summary of various strategies for PSC self-healing.

Type	Self-healing condition	PSC architectures	PCE [%] (control PCE)	Method	Recovery	Ref.
Immobilization of decomposed species	Stored for 10 h in the dark under N_2 atmosphere	ITO/$PC_{61}BM$/AZO/$MAPbI_3$/NiO_x/FTO /glass	–	Prevent Ag diffusion into perovskite by substituting Ag electrode with ITO electrode	90% of its initial value after 17 cycles (one cycle: harvesting–rest–recovery)	[108]
	Stored for 12 h in dark	Au/spiro-OMeTAD/PDMS-borax+ $(FAPbI_3)_{0.95}(MAPbBr_3)_{0.05}$ /SnO_2/FTO/glass	22.05 (best) 20.70 (aver.) (20.93, 19.22)	Prevent escape of decomposed species and react w/PbI_2 to regenerate perovskite	~95% of its initial value after two cycles (one cycle: 10 h working–12 h recovery)	[110]
	Maintained in ambient air for 45 s	Au/spiro-OMeTAD/PEG + $MAPbI_3$/TiO_2/ FTO/glass	12.5 (aver.) (~8)	Prevent escape of MAI by strong interaction between MAI and PEG	Recover *J*–*V* curve almost to its original value	[111]
	Maintained in ambient air for 30 s	Au/spiro-OMeTAD/PVP + $MAPbI_3$ /m-TiO_2/c-TiO_2/FTO/glass	20.32 (best) (18.47)	Prevent escape of MAI by strong interaction between MAI and PVP	50% of its initial value after three cycles (one cycle: water spraying 60 s–repair 30 s)	[112]
	Stored for 2 h under N_2 atmosphere without heat and light	1*H*,1*H*,2*H*,2*H*-perfluorodecyltrichlorosilane (FDTS) /Al_2O_3/Ag/PCBM/$MAPbI_3$/NiO/ITO /glass	19.7 (best) (19.9)	Prevent escape of gaseous products from perovskite decomposition by encapsulation	Recover *J*–*V* curve almost to its original value	[113]
Redox of Pb^0 and I^0 defects	Soaked in ferrocene (Fc) solution for 12 h	Au/spiro-OMeTAD /$MAPbI_3$/SnO_2/FTO/glass	16.9 (best) (–)	Recover elemental defects by chain-reaction cycle of Fc → FcI → $FcPbI_3$ → Fc	16.0% of PCE after recovery (pristine: 16.9%, decomposed: 14.9%)	[114]
	–	Au/spiro-OMeTAD /Eu^{3+}+(FA, MA, Cs) Pb (I, Br)$_3$(Cl)/TiO_2/ITO	21.52 (best)	Redox shuttle selectively oxidized Pb^0 and reduced I^0 defects by Eu^{3+}-Eu^{2+}_ redox shuttle	2.7% of Pb^0/(Pb^0+Pb^{2+}) after 85 °C 1000 h (pristine: 11.3%)	[115]
Self-healing polymer	Stored for 2 h at RT	PDMS/hc-PEDOT:PSS/PCBM /$FAPbI_3$/PEDOT:PSS /hc-PEDOT:PSS /PDMS	19.50 (best) (16.57)	Prevent moisture by hydrophobic polysiloxane (SHP) and passivation of fragile grain boundary	80% of its initial value after 800 cycles (1 cycle: stretching with 20% strain–rest)	[116]
	Thermal annealing at 80 °C for 10 min	Ag/PEI/$PC_{61}BM$/polyurethane elastomers with disulfide bonds (PUDS) + $MAPbI_3$ /NiO_x/ITO/PEN	17.19 (best) (–)	Thermally driven self-healing of cracked perovskite by PUDS polymer	80% (13.71% PCE) of its initial value after two cycles (One cycle: bending–heal) (pristine: 17.19%, cracked: 2.06%)	[117]
	Thermal annealing at 100 °C for 10 min	PDMS/hc-PEDOT:PSS/PEDOT:PSS /PEI/PCBM/self-healing polyurethanes (s-PU) + $MA_{0.22}FA_{0.78}PbBr_{0.03}I_{0.97}$ /PEDOT:PSS/hc-PEDOT:PSS /PDMS	19.15 (best) 18.68 (aver.) (14.74, 14.06)	Thermally driven self-healing of cracked perovskite by s-PU polymer	88% of its initial value after 1000 cycles (1 cycle: 20% stretching–100 °C annealing)	[118]
	Thermal annealing at 85 °C for 30 min	Ag/BCP/$PC_{61}BM$ /thiourea-triethylene glycol polymer (TUEG3) + $MAPbI_3$/PTAA/PH1000 /ITO/PET	8.87 (best) 6.46 (aver.) (13.69, 11.35)	Thermally driven self-healing of cracked perovskite by TUEG3 polymer	80% of its initial value after 1.5 mm radius 50 times bending–85 °C annealing step	[119]

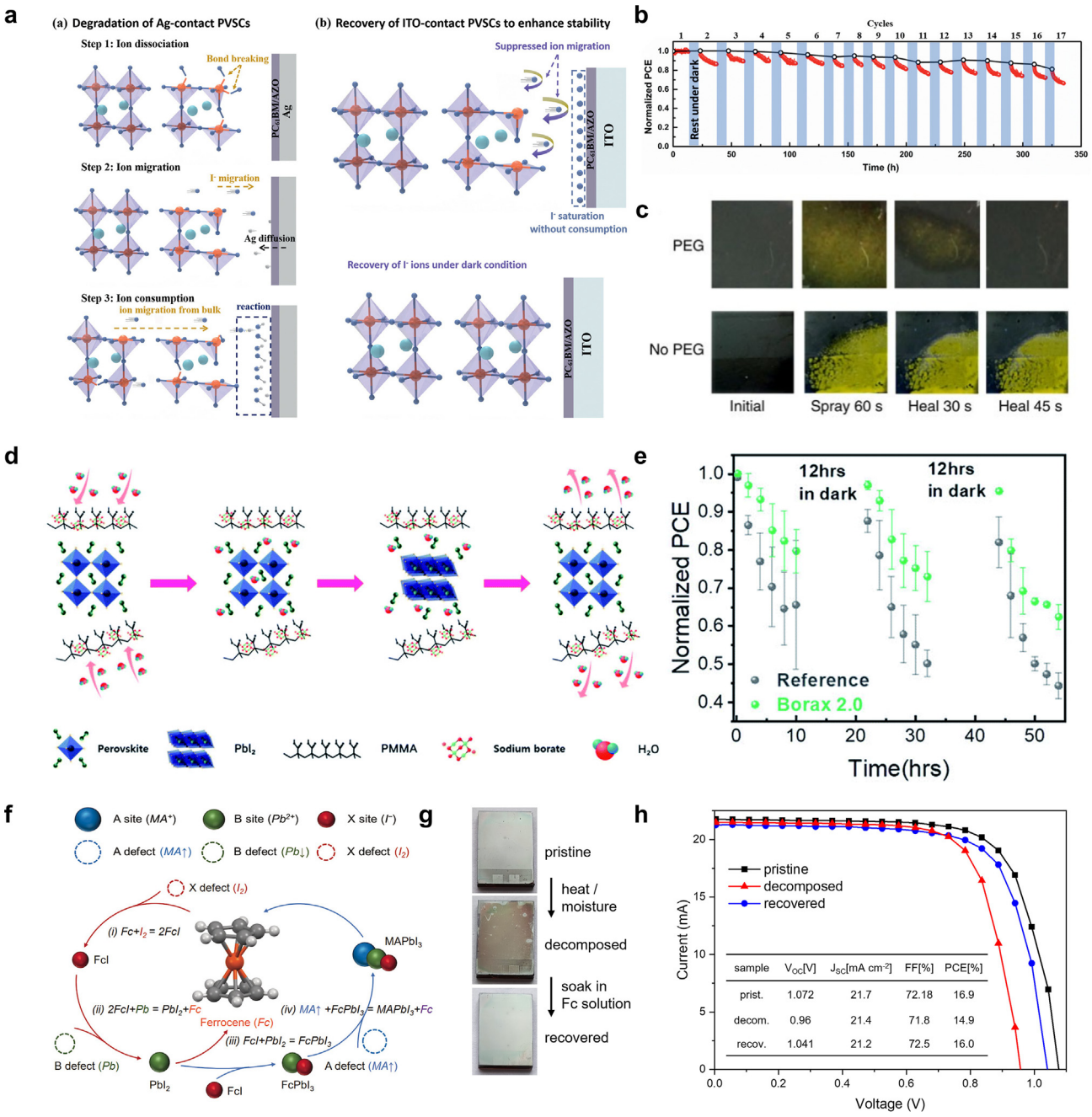

Fig. 7. (a) Schematic illustration of the degradation and recovery processes involving ion migration; and (b) self-healing performance achieved by dark storage. Reproduced from Ref. [108]. Copyright 2021 Wiley-VCH. (c) Optical images showing surface changes on perovskite films without/with PEG (60 s water spraying and 45 s in ambient air). Reproduced from Ref. [111]. Copyright 2016 Springer Nature. (d) Self-healing process by PMMA treatment and (e) the self-healing performance results. Reproduced from Ref. [110]. Copyright 2022 Royal Society of Chemistry. (f) Sustainable self-healing process via Fc/Fc^{+} redox shuttle. (g) Photographs and (h) PSC *J–V* curves during Fc-assisted self-healing. Reproduced from Ref. [114]. Copyright 2021 Wiley-VCH.

overcoming the lower PCE remains critical for practical use, underscoring the necessity of recycling the metal electrode.

4.1.1. *Substrate recycling*

The TCO substrate accounts for a significant portion (> 43%) of the overall cost of PSC fabrication (Fig. 10a) [132,134]. Additionally, such substrates involve rare resources (e.g., tin and indium), which further limit the commercialization of PSCs. Initially, TCOs were recycled because of their stability and simple recovery process compared to other PSC components. TCOs can be easily recovered by dissolving their upper layers (e.g., ETL, perovskite, and HTL; Table 5). A layer-by-layer approach to TCO recycling was demonstrated by selectively stripping the upper layers (Fig. 10b) [134]. First, the gold electrode was removed using adhesive tape, followed by the removal of spiro-OMeTAD by immersion in chlorobenzene. Subsequently, the perovskite layer was transformed into PbI_2 through water treatment; PbI_2 was then removed by immersion in DMF, resulting in the recovery of TiO_2/FTO/glass. However, the recycled PSC exhibited a significant decrease in PCE, which was attributed to TiO_2 degradation during DMF immersion. Thus, the TiO_2 layer was further immersed in DMF to remove it from the substrate, resulting in the recovery of FTO/glass. Notably, although TiO_2 is insoluble in DMF, solvent penetration into the TiO_2 pores potentially causes delamination of the TiO_2 layer. The recycled PSCs fabricated using the recovered TCO substrate exhibited a PCE (15.1%) comparable to that

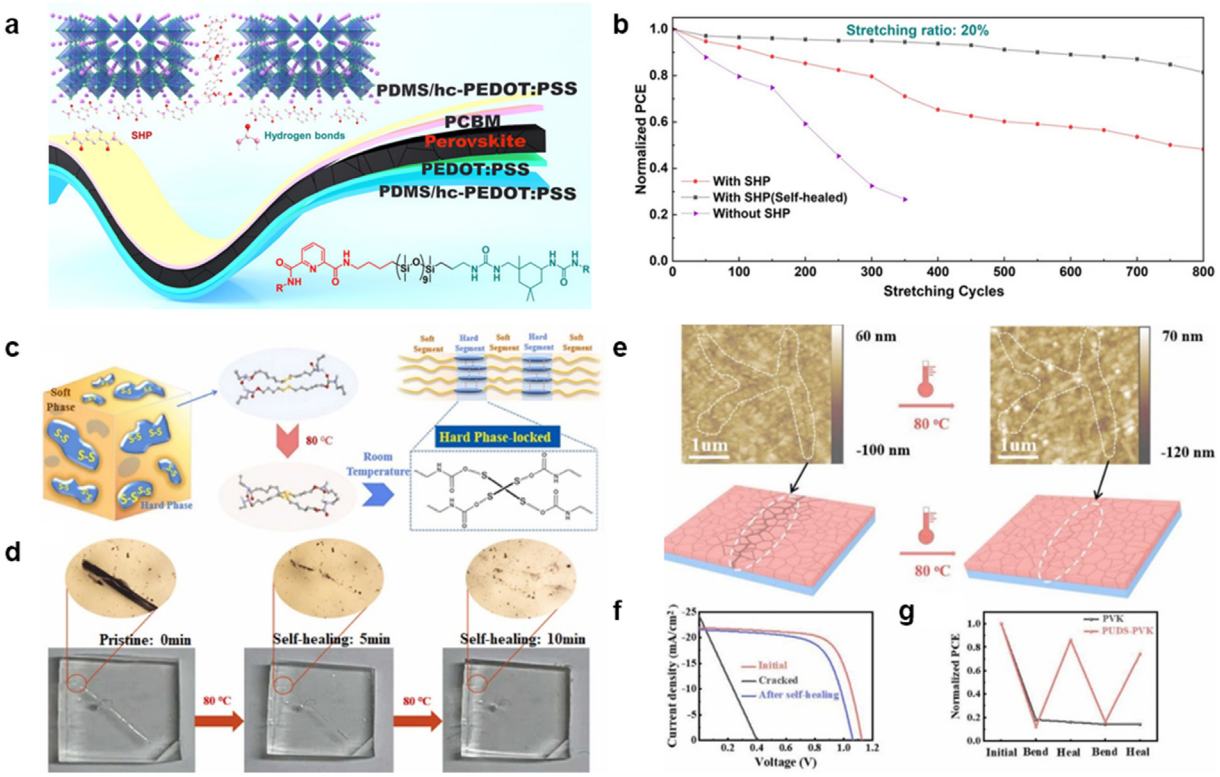

Fig. 8. (a) Schematic illustration of passivation and self-healing mechanisms via SHP and (b) self-healing performances of flexible PSCs with/without SHP during the stretching cycles under 20% strain. Reproduced from Ref. [116]. Copyright 2022 Wiley-VCH. (c) Schematics of the self-healing process by PUDS and (d) optical images of PUDS during the crack self-healing process. (e) AFM images and illustrations of the cracked and self-healed perovskite films. (f) *J–V* curves of flexible PSCs under the crack and self-healing process and (g) self-healing cycle test. Reproduced from Ref. [117]. Copyright 2022 Elsevier.

(14.6%) of the fresh PSC (Fig. 10c). A similar approach was introduced for recycling major components such as Au, Pb, and TCO substrates [135]. PSC dismantling involved sequential immersion in chlorobenzene, ethanol, and DMF, leading to the recovery of Au, Pb, and TiO_2/FTO/-glass. The recycled PSCs using the recovered TiO_2/FTO/glass achieved PCEs of 15–16%, indicating no significant decline in photovoltaic performance after recycling. The slight decrease in PCE was attributed to a reduction in J_{sc}, potentially caused by residual solvents during the recycling process. Although the photovoltaic performance post-recycling of Au/Pb was not demonstrated, the recovery of each valuable component through a sequential dismantling process for recycling was demonstrated, indicating the potential to reduce the fabrication cost and environmental impact of PSCs. Kim *et al.* conducted a study to identify an appropriate solvent for recycling TCO from PSCs (Fig. 10d) [136]. The *J–V* curves of the PSCs fabricated with fresh PbI_2 revealed that polar solvents dissolved the perovskite layer, whereas non-polar solvents only removed the spiro-OMeTAD layer. However, the dissolution kinetics of polar protic solvents (ethanol and water) were slow (~24 h), owing to the low solubility of metal halides. Conversely, polar aprotic solvents effectively decomposed the perovskite layer within a brief time (within 30 s) through a reaction between the partially negative aprotic solvents and Pb^{2+} ions in the perovskite. The TiO_2/FTO/glass recovered using a polar aprotic solvent exhibited optical characteristics similar to those of fresh TiO_2/FTO/glass and showed a PCE comparable to that of PSCs fabricated using a fresh substrate. Moreover, this recycling process demonstrated multiple repeatability, maintaining the initial PCE (15%) even after 10 cycles (Fig. 10f). Likewise, Huang *et al.* recycled FTO/glass substrates from ETL-free PSCs using DMF, achieving a comparable PCE of ~10% with the recycled substrates [137]. They also demonstrated the recycling of TiO_2/FTO/glass using the same procedure, achieving a slightly decreased PCE of 11.87% for the recycled PSCs compared to the 14.08% observed with fresh PSCs [138]. This reduction in PCE was attributed to a decrease in the fill factor, owing to a reduction in the shunt resistance (R_{sh}) and an increase in the series resistance (R_s). The decrease in R_{sh} was attributed to the altered surface affinity of the substrate, which facilitated direct contact between the ETL and HTL in local areas. Meanwhile, the increase in R_s was attributed to surface modifications of c-TiO_2, owing to residual materials and changes in the surface topography resulting from multiple cleaning procedures.

Alternative solvents for recycling TCO substrates have been explored. One approach is the use of a single non-volatile cost-effective alkaline solvent to recover the TCO substrate [139]. To recover ITO/glass, the effects of different KOH concentrations on the recovered substrates were investigated (Figs. 11a–d). The ITO/glass recovered using 1.5 M KOH showed optical transmittance and electrical uniformity comparable to those of the fresh ITO substrate, whereas a lower KOH concentration resulted in residues/impurities on the substrate that could impact the surface properties. Additionally, KOH treatment enhanced the substrate wettability, leading to a high fill factor. Consequently, the recycled PSCs exhibited a PCE (7.20%) similar to that of fresh PSCs (8.05%). Alkylamines (butylamine, dipropylamine, diethylamine, and dibutylamine) have also been investigated as solvents for recycling TCO substrates from inverted PSCs [141]. NiO_x/ITO/glass was recovered using a two-step process involving two alkylamine solvents (Figs. 11e–g). Notably, the substrate recovered through butylamine–dipropylamine treatment exhibited a high PCE (20%), surpassing that of the fresh PSCs (17.92%). This enhanced PCE was attributed to the strong alkylamine–NiO_x interactions, resulting in Ni–N coordination. This interaction enhances photovoltaic performance by passivating defects and providing a template effect for perovskite crystallization. Furthermore, the recycled PSCs maintained their photovoltaic performance even after 10 re-cycles, demonstrating the practicality and potential of this approach for recycling high-quality substrates from PSCs.

Although significant progress has been made in recycling TCO substrates, several challenges must still be addressed for the sustainable commercialization of PSCs. In particular, it is important to consider the

Table 4
Reported PSC rejuvenation strategies and photovoltaic performances.

PSC architectures	Reuse methods	Reused architectures	Reuse time	PCE [%]	Ref.
Au/spiro-OMeTAD/$MAPbI_3$ /ZnO/ITO/glass	Immersion in MAI solution and heat treatment	Au/spiro-OMeTAD/$MAPbI_3$/ZnO/ITO/glass	0	11.59	[125]
			1	11.59	
			2	11.04	
Au/PTAA/$MAPbI_3$/TiO_2 /FTO/glass	Spin coating of MAI solution and heat treatment	Degraded perovskite/TiO_2/FTO/glass	0	16.8	[126]
			1	7.6	
Ag/spiro-OMeTAD /$MAPbI_3$/m-TiO_2 /c-TiO_2/FTO/glass	HTM dissolution by CB and thermal decomposition of $MAPbI_3$ and spin coating of MAI solution	PbI_2/ETM/FTO/glass	0	14.35	[127]
			1	14.84	
			2	8.51	
Au/spiro-OMeTAD /$MAPbI_3$/TiO_2/FTO/glass	HTM dissolution by CB and thermal decomposition of $MAPbI_3$ and spin coating of MAI solution	PbI_2/ETM/FTO/glass	0	16 <	[128]
			1	14–15	
Carbon/$MAPbI_3$/m-ZrO_2 /m-TiO_2/c-TiO_2/FTO/glass	Introduction of methylamine gas	Carbon/$MAPbI_3$/m-ZrO_2/m-TiO_2/c-TiO_2/FTO/glass	0	14.39	[129]
			1	≈12	
			2	≈13	

recycling of various materials in conjunction with TCO substrates and carefully evaluate the cost and environmental impact of the entire recycling process.

4.1.2. *Metal electrode recycling*

Noble metal electrodes, particularly Au electrodes, used in PSCs are expensive. Despite the relatively small number of PSCs, their reuse is crucial for practical large-scale applications. Therefore, recycling metal electrodes is necessary to address the cost and sustainability concerns in the PSC industry. Similar to TCO/substrate recycling, metal electrodes can be easily separated and recycled by immersion in a solvent that decomposes the perovskite layer. An early study revealed that the Au electrode recovered through immersion in DMF contained only 0.41% Pb impurities, indicating its potential for facile Au recycling [136]. Another approach involved layer-by-layer dissolution for recovering Au, which showed no traces of foreign metals [135]. However, for their desired application, these recovered Au electrodes may require additional processes such as purification, deposition, and manufacturing, thereby increasing costs and environmental impacts. Yang *et al.* developed a recycling process for Au electrodes using a dry transfer process, which allowed the direct redeposition of the Au electrode onto a newly fabricated HTL (Fig. 12) [133]. To facilitate the simple fabrication and recycling process, they employed a nanoporous Au electrode of high specific surface area, which enabled effective contact with the HTL. In this process, the PSCs were immersed in acetone to dissolve the perovskite layer and HTL. The floating nanoporous Au electrode was then transferred onto a membrane film for reuse. After washing, the nanoporous Au electrode on the membrane was directly attached to the HTL, and the membrane film was slowly detached. This process could be repeated multiple times, and the PCE of the recycled PSCs comprising the nanoporous Au electrode maintained its performance even after 12 cycles, demonstrating the feasibility of reducing fabrication costs, minimizing resource wastage, and reducing environmental impact. However, the loss and cracking of the Au electrode during the recycling process and the limitations in device size need to be overcome.

4.2. *Toxic materials recycling*

Environmental concerns surrounding PSCs have led to extensive investigations into the potential toxicity risks posed by hazardous substances. LCA studies have been conducted to quantitatively assess environmental impacts and develop more effective and sustainable PSC technologies [8,143–145]. Recent LCAs have demonstrated that recycling strategies can reduce greenhouse gas emissions by up to 71.2% and decrease energy payback time by up to 72.6% [8]. In particular, the main perovskite component, Pb, presents a challenging obstacle for commercialization owing to its toxicity. Consequently, the Pb in the perovskite adsorption layer has been substituted with Sn; however, Sn-based PSCs showed lower PCEs and stability [146–148]. Moreover, several reports have indicated that replacing Pb is not an effective solution because of the tradeoff between hazardous effects and reduced PCE and stability [149–151]. The utilization of toxic solvents in the recycling process is another key limiting factor for commercialization. Therefore, solvent recycling is important in the implementation of sustainable recycling technologies for the commercialization of PSCs.

4.2.1. *Pb recycling*

The solubility and purity issues associated with PbI_2, which serves as a precursor for refabricated perovskite layers, makes the recycling of Pb in PSCs challenging. The Pb recycling process typically involves dissolving the perovskite and extracting the Pb. Various solvents have been employed to dissolve perovskites, including deep eutectic and polar aprotic solvents (Table 6). Polar aprotic solvents (DMF, γ-butyrolactone, and DMSO) have been mainly utilized because they can easily dissolve the perovskite layer through the reaction between their partially negative O and positive Pb cations [136]. DMF has been extensively studied and employed as a representative polar aprotic solvent. Binek *et al.* employed DMF to dissolve PbI_2 after sequentially removing the HTM and MAI layers from PSCs using chlorobenzene and water, respectively [134]. The recycled PbI_2 was used to fabricate PSCs that exhibited an efficiency exceeding 12%, which is comparatively lower than that of the PSCs prepared with fresh PbI_2 (14.6%). The decrease in PCE resulting from a reduction in the open-circuit voltage and fill factor were attributed to impurities in the PbI_2 solution. Another approach for recycling Pb from carbon-based PSCs was demonstrated, which does not require the removal of the HTM owing to its HTM-free structure [152]. The carbon-based PSC was immersed in DMF and the dissolved Pb was precipitated with NH_3H_2O to form $Pb(OH)_2$. Subsequently, by adding HI solution, yellow PbI_2 powder was obtained, which exhibited a high recovery rate of 95.7%; it was then used to refabricate PSCs. The PCE of the recycled PSCs was lower (11.36%) than that of the original PSC (12.17%). This reduction was ascribed to impurities introduced during the precipitation process, emphasizing the significance of high-purity recycled PbI_2. Other approaches to Pb recycling involve adsorption processes, which can enhance the Pb selectivity and consequently improve the purity of the recycled Pb compounds. Kim *et al.* reported the recovery of Pb from DMF solutions containing perovskites using HAp ($Ca_{10}(PO_4)_6(OH)_2$) as the adsorbent [136]. Park *et al.* recently developed a Pb-recycling process using Fe-decorated HAp (HAp/Fe) [153]. HAp/Fe was employed to adsorb Pb from the DMF solution containing the dissolved perovskite, and the Pb-adsorbed HAp/Fe could be easily collected using a magnetic field (Fig. 13a). Subsequently, Pb was recycled as PbI_2 for the fabrication of PSCs through acid treatment to dissolve HAp/Fe and precipitate PbI_2. The decorated Fe not only exhibited magnetic properties for efficient collection, but also provided high adsorption sites, resulting in an impressive 99.97% recovery rate (Fig. 13b). Additionally, the recycled PSCs achieved a PCE (16.04%) comparable to that (16.65%) of fresh PSCs, indicating their potential for Pb emission-free PSC

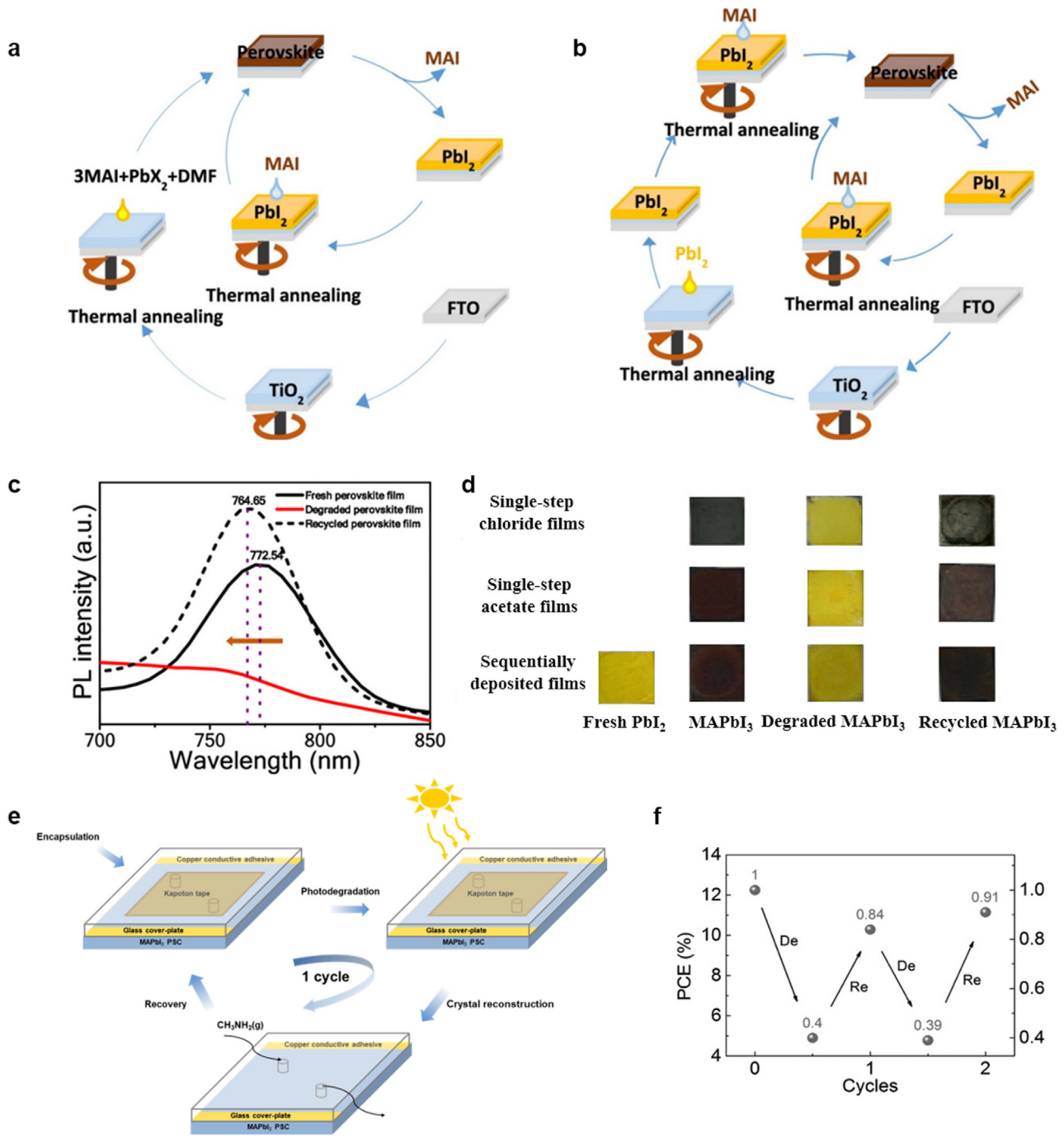

Fig. 9. Illustration of the recycling process by (a) single-step and (b) sequential deposition route. (c) PL spectra of $MAPbI_3$ film deposited by single-step acetate routes, and (d) optical images of perovskite films via different recycle processes. Reproduced from Ref. [130]. Copyright 2019 American Chemical Society. (e) Schematic illustration of degradation–regeneration cycle for encapsulated PSCs and (f) their corresponding PCEs during two cycles. Reproduced from Ref. [129]. Copyright 2017 Wiley-VCH.

manufacturing (Fig. 13c). Pb recycling can be conducted using various adsorbents, including metal oxides [154,155], carbons [156,157], biosorbents [158,159], and ion exchange resin [103,160], and the recycling characteristics can vary depending on the type of adsorbent used. Hong *et al.* reported the Pb recycling performance using two different biosorbents, HAp and whitlockite ($Ca_{18}Mg_2(HPO_4)_2(PO_4)_{12}$ (Fig. 13d) [158]. Despite having similar compositions, they showed different adsorption mechanisms, which affected the Pb recycling performance. Indeed, whitlockite exhibited a higher Pb adsorption capacity (2339 mg/g) than HAp (239 mg/g) because of its dissolution–reprecipitation Pb removal mechanism (Fig. 13e). Furthermore, the complete transformation of whitlockite into hydroxypyromorphite ($Pb_{10}(PO_4)_6(OH)_2$) allowed to produce high-purity PbI_2, resulting in a comparable PCE of 19.00% for recycled PSCs (fresh PSC PCE: 19.31%; Fig. 13f). Conversely, the recycled PSCs using HAp exhibited a relatively low PCE (16.85%), indicating that the PbI_2 purity significantly impacts the performance of recycled PSCs. Cation-exchange resins were also employed by Chen *et al.* for low-cost Pb recycling [140]. The PSCs were first dissolved in DMF,

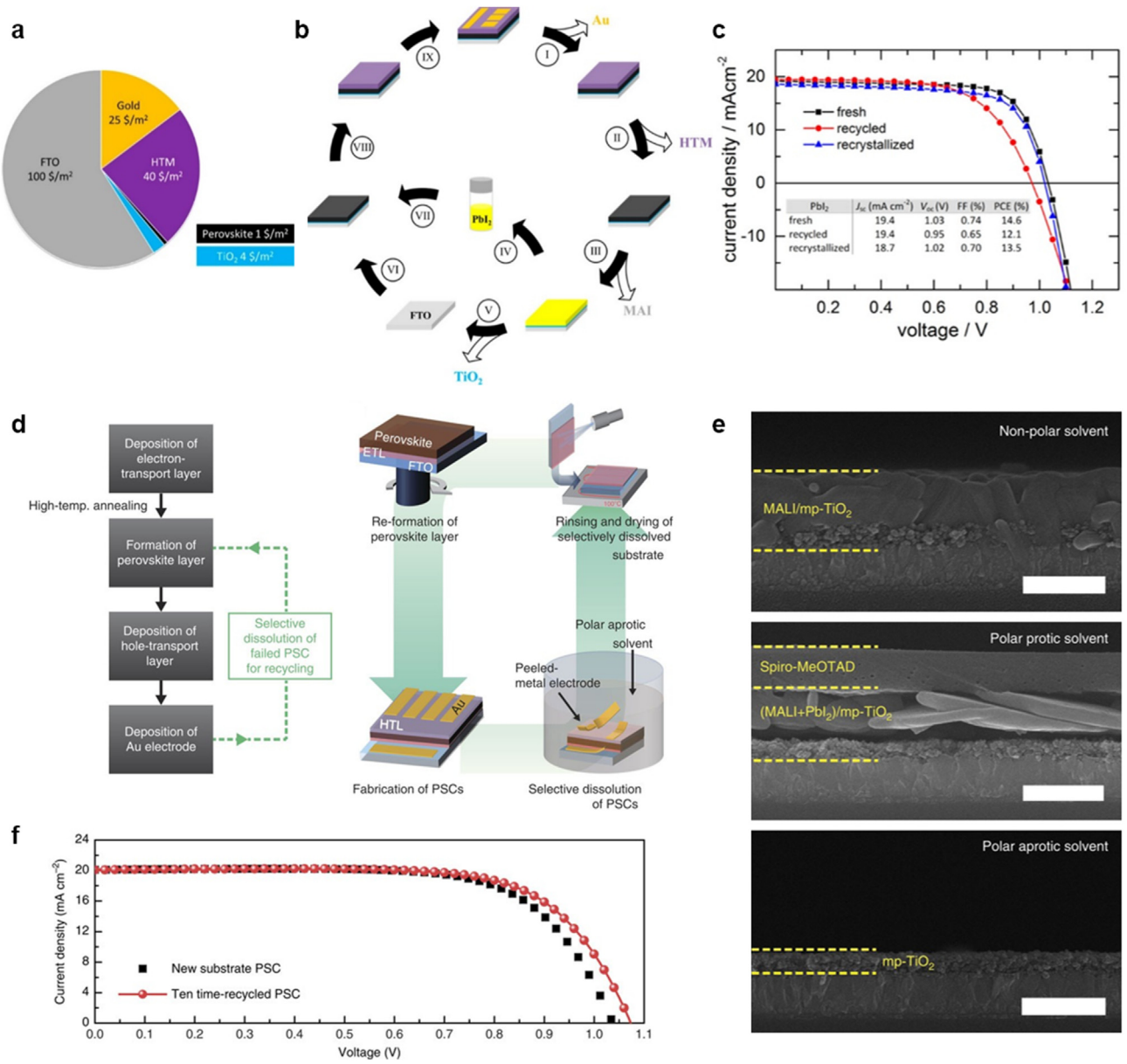

Fig. 10. (a) Pie chart of the estimated cost of each PSC layer. (b) Recycling process of PSCs: (I) Ag electrode removal by adhesive tape, (II) HTM removal by immersion in chlorobenzene, (III) MAI extraction in water, (IV, V) PbI_2 and TiO_2 removal using DMF, (VI) coating of new TiO_2 layer, (VII) preparation of the perovskite layer on recycled FTO, (VIII) coating of new HTM layer, and (IX) deposition of Au electrode. (c) *J–V* curves of PSCs fabricated with fresh, recycled, and both recycled and recrystallized PbI_2. Reproduced from Ref. [134]. Copyright 2016 American Chemical Society. (d) Recycling procedures for PSCs and their schematic illustration. (e) Cross-sectional SEM images of PSCs treated with different solvent types. (f) *J–V* curves of PSCs fabricated with fresh and tenfold-recycled substrates. Reproduced from Ref. [136]. Copyright 2016 Springer Nature.

and the Pb ions were fully adsorbed using a carboxylic acid cation-exchange resin. The Pb ions could be easily released as $Pb(NO_3)_2$ in an HNO_3 aqueous solution because of the weak carboxylic acid group, resulting in a high Pb recycling efficiency of 99.2%. Subsequently, $Pb(NO_3)_2$ was transformed into PbI_2, demonstrating a photovoltaic performance comparable to that of PSCs fabricated using high-purity (99.99%) commercial PbI_2. Additionally, the material cost for the recycling process was \$1.35/m^2, assuming fivefold reuse of DMF and resin, thereby leading to energy and cost savings comparable to PSC fabrication using new materials. Despite these positive progresses for Pb recycling using adsorbents, significant issues regarding the use of toxic solvents remain. Poll *et al.*, demonstrated the use of a DES for recycling Pb from PSCs [161]. The DES, consisting of ChCl and EG, effectively dissolved the perovskite layers in PSCs, allowing for the subsequent electrodeposition of Pb with a 99.8% recovery rate. An advantage of using DES over aqueous solvents is the reduced risk of contaminating the water supply with waste solutions. Additionally, DES does not require volatile organic solvents or concentrated acids, making it a more environmentally friendly option. Recently, molten LiCl–KCl was employed to dissolve PbI_2 from perovskite, followed by electro-extraction of Pb metal and I_2 products [162]. This method achieved a 99.89% Pb recovery rate at a lower cost (~\$8.9/kg Pb) compared with that achieved in previous studies (\$10–\$160/kg Pb). Despite these advantages, the electrochemical deposition process to obtain the desired Pb can be complex under practical working conditions, and additional steps are required for the reuse of the recovered Pb in PSC fabrication because of its recovered solid form. Deng *et al.* demonstrated a simplified Pb recycling process using evaporation methods, eliminating various steps including adsorption, adsorbent dissolution, precipitation, and electrodeposition (Fig. 13g) [163]. In this approach, PSCs were dissolved in a DMF/DMSO solvent mixture and

Table 5
Reported substrate recycling strategies and photovoltaic performances of PSCs.

Architectures	Recycled Materials	Recycling time	PCE [%]	Ref.
Ag/spiro-OMeTAD/$MAPbI_{3-x}Cl_x$/FTO/glass	FTO/glass	0	11.82	[137]
		1	10.81	
		2	9.97	
Au/spiro-OMeTAD/$MAPbI_3$/TiO_2/FTO/glass	FTO/glass	0	14.6	[134]
		1	15.1	
		3	15.4	
Au/spiro-OMeTAD/$MAPbI_3$ or $(FAPbI_3)_{0.85}(MAPbBr_3)_{0.15}$ /TiO_2/FTO/glass	TiO_2/FTO/glass	0	15	[136]
		10	> 15	
Ag/spiro-OMeTAD/$MAPbI_{3-x}Cl_x$/m-TiO_2 / FTO/glass	mp-TiO_2/FTO/glass	0	14.08	[138]
		1	12.67	
		2	11.87	
Ag/spiro-OMeTAD/$MAPbI_3$/c-TiO_2/FTO/glass	c-TiO_2/FTO/glass	0	14.79	
		1	12.60	
		2	11.03	
Au/spiro-OMeTAD/$MAPbI_3$/TiO_2/FTO/glass	TiO_2/FTO/glass	0	16.1	[135]
		1	16.0	
		2	15.0	
Al/Ca/$PC_{60}BM$/$MAPbI_3$/TiO_2/PEDOT:PSS/ITO /glass	ITO/glass	0	8.15	[139]
		1	7.20	
Cu/Cr/C_{60}BCP/$Cs_{0.1}FA_{0.9}PbI_3$/PTAA/ITO/glass	ITO/glass	0	16.6	[140]
		1	15.5	
Ag/PCBM/CsFAMA/NiO_x/ITO/glass	NiO_x/ITO/glass	0	17.92	[141]
		1	20	
Au/spiro-OMeTAD/$MAPbI_3$/ZnO/AZO/glass	ZnO/AZO/glass	0	13.5	[142]
		1	12.6	
Au/spiro-OMeTAD/$MAPbI_3$/ZnO/AZO/PET	ZnO/AZO/PET	0	7.2	
		1	6.8	

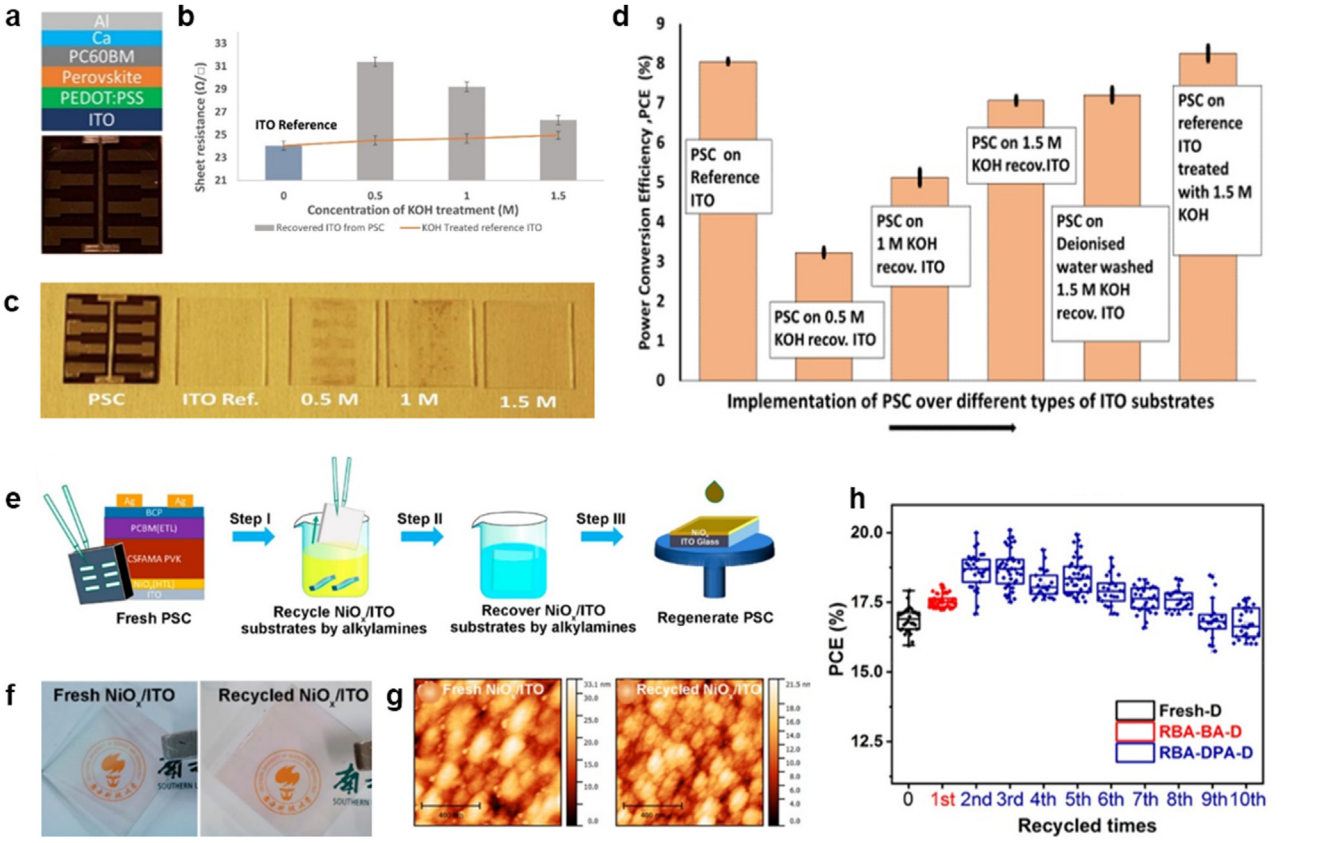

Fig. 11. (a) PSC structure and its corresponding optical image. (b) Sheet resistance and (c) optical images of ITO substrates treated with various KOH concentrations. (d) PCE of PSCs fabricated with reference and ITO substrates treated with different KOH concentrations. Reproduced from Ref. [139]. Copyright 2019 Elsevier. (e) Schematic recycling process of substrates using alkylamines. (f) Optical images and (g) AFM surface morphologies of the fresh and recovered substrates. (h) PCE of PSCs fabricated with fresh (Fresh-D) and recycled substrates using various alkylamines (benzyl alcohol–benzyl alcohol treatment: RBA-BA-D, benzyl alcohol–dipropylamine treatment: RBA-DPA-D). Reproduced from Ref. [141]. Copyright 2021 American Chemical Society.

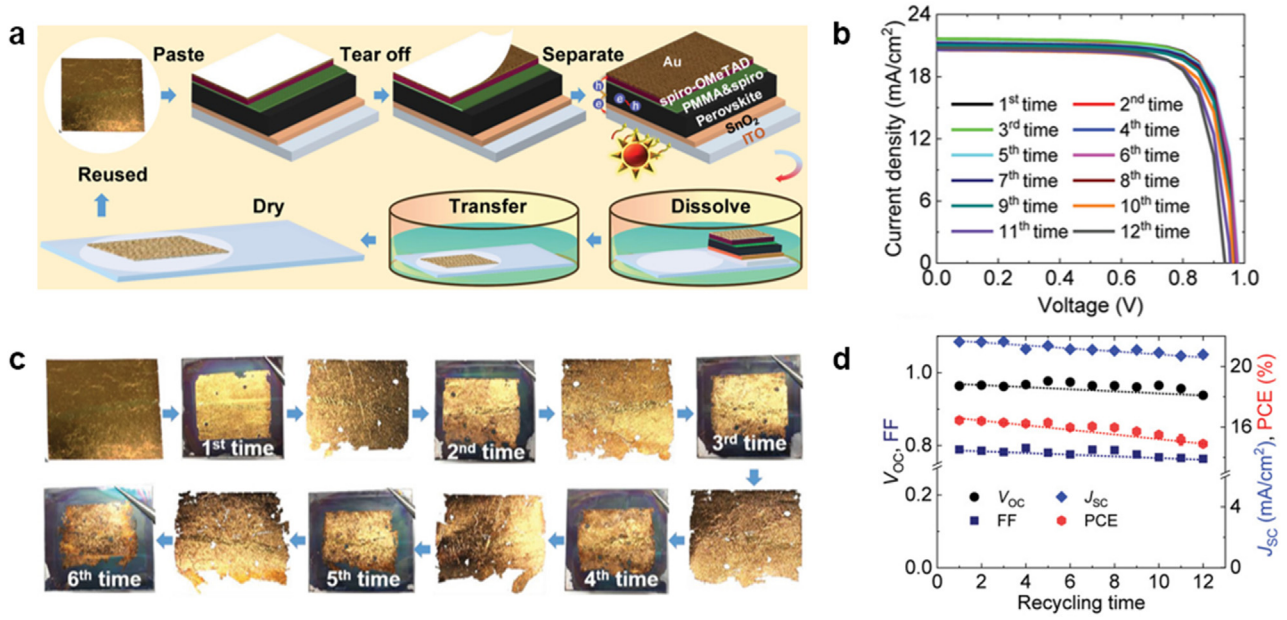

Fig. 12. (a) Schematic illustration of the Au electrode recycling procedure. (b) *J–V* curves of PSCs fabricated using a multi-recycled Au electrode. (c) Optical images of Au films during the sixth recycling process and (d) photovoltaic parameters of PSCs fabricated with multi-recycled Au electrodes. Reproduced from Ref. [133]. Copyright 2020 Wiley-VCH.

subsequently evaporated at 100 °C. The resulting yellow powder mainly consisted of PbI_2 with a small amount of MAI, which is consistent with the reported degradation progress of perovskite into PbI_2. The recovered PbI_2 powder was then reused as a perovskite precursor, thereby achieving a slightly reduced PCE of 15.30% for a single recycling process (fresh PSC PCE: 16.29%; Fig. 13h). Although this recycling strategy provides a simplified process and reduces costs and harmful effects, the use of DMF/DMSO during the perovskite dissolution process still poses environmental concerns. More recently, Schmidt *et al.* introduced a novel approach for PbI_2 recycling utilizing a solvent-free method based on hot water extraction [164]. They observed that the solubility of PbI_2 in water was more temperature-sensitive than that of other halide salts, including CsI, MAI, FAI, and CsCl. While these salts remain highly soluble even at 20 °C, the PbI_2 solubility exceeds 1 g/L at temperatures > 50 °C. Based on this difference, the perovskite was dissolved in water at 50 °C, whereby only PbI_2 recrystallized during the subsequent cooling process while the other salts remained in solution. This process yielded crystalline PbI_2 with a remarkable purity > 95.9%, resulting in a 94.4 ± 5.6% PB recovery rate. Although this method significantly alleviates environmental concerns during recycling, the purity level required for direct reuse in PSC fabrication remains a concern; therefore, further studies are required to address this issue.

4.2.2. *Solvent recycling*

Another critical issue is the use of toxic solvents in the PSC recycling process. DMF, DMSO, and chlorobenzene are commonly used in this process because they easily dissolve the perovskite/CTL. However, these solvents are classified as hazardous or problematic substances that can affect safety, health, and the environment, making it necessary to recycle or manage them during the entire recycling process [168]. Notably, the reuse of solvents in the recycling process has rarely been reported. Chen *et al.* demonstrated the possibility of reusing DMF multiple times in the recycling process [103]. Similarly, the reuse of water in hot-water extraction for Pb recycling has been reported for other Pb extractions [164]. However, in practical applications, an increase in the number of water reuse cycles may lead to excess iodide concentration, which can limit the Pb^{2+} solubility and reduce the Pb yield. Therefore, further research is necessary to determine the maximum number of times the extraction process can be repeated, and to assess the cost and environmental implications associated with these treatment methods. In recent years, a "one-key-reset" recycling strategy has been implemented, which considers the environmental impact of both the fabrication and recycling processes (Fig. 14) [167]. In this method, the perovskite and spiro-OMeTAD components are simultaneously dissolved using a bleaching solution to form two separate liquid phases (liquefied perovskite and spiro-OMeTAD dissolved THF). Subsequently, each liquid is collected and reused as a precursor to fabricate new PSCs. The refabricated PSCs exhibited a high PCE exceeding 20%, indicating the potential of this approach as a sustainable PSC recycling method. Nonetheless, additional research is necessary to address the composition uncertainty of the recycled liquids. Recently, there have been reports on the reuse of toxic solvents in the recycling process of PSCs [14]. In a two-step dissolution process, PSCs were separated, and the recovered solvents, chlorobenzene and DMF, were reused as solvents for perovskite precursor. PSCs fabricated with these recovered solvents exhibited a remarkable PCE of 25.02%, comparable to that of control PSCs (25.12%), indicating the potential for a sustainable recycling strategy. However, additional research is needed to analyze in detail the residual organic and halide components in the recovered solvent and manage the residual components for the pure solvent recycling. In addition, to establish a sustainable closed-loop PSC industry, comprehensive investigations and discussions regarding the recycling of residual solvents during PSC fabrication are crucial.

5. Conclusion and outlook

5.1. *Long-term stability*

Stability enhancement is critical in the development of PSCs to overcome their vulnerability to degradation by environmental factors. Various strategies, including metal electrode optimization, internal stress control, additive incorporation, interfacial bilayers, and 2D perovskite layers, have shown promising results in improving stability and overall performance. Additives with functional groups can effectively passivate surface defects, inhibit ion migration, and enhance stability. Interfacial bilayers provide defect passivation and protection against external factors, thereby contributing to long-term stability. The implementation of

Table 6
Reported Pb recycle strategies and photovoltaic performances of PSCs.

PSC architectures	Recycle methods	Dissolving solvent	Pb recovery rate [%]	Recovered form	Re-cycling time	PCE [%]	Ref.
$MAPbI_3$, $FAPbI_3$, or $MAPb_{3-x}I_x$ /TiO_2/FTO/glass	Dissolution and electrodeposition	DES (ChCl-EG)	99.8	Pb	–	–	[161]
Degraded PSCs (no structural information)	Dissolution and electrodeposition	DES (LiCl–KCl)	99.89	Pb, I_2	–	–	[162]
Au/spiro-OMeTAD/$MAPbI_3$/TiO_2/FTO /Glass	Dissolution and precipitation	chlorobenzene, water, DMF	– 92–94	PbI_2	0 1	14.6 12.1	[134]
Carbon/$MAPbI_3$ /m-TiO_2/c-TiO_2/FTO /Glass	Dissolution and precipitation	DMF	– 95.7	PbI_2	0 1	12.17 11.36	[152]
Ag/spiro-OMeTAD /$MAPbI_{3-x}Cl_x$/FTO /Glass	Dissolution, precipitation, and adsorption	DMF	99.98–99.99	Pb	–	–	[136]
Ag/BCP/PCBM /$MAPbI_3$/NiO_x/ITO /Glass	Dissolution and precipitation	butyl amine, toluene, EtOH	– 98.9	PbI_2	0 1	17.84 17.95	[165]
Au/spiro-OMeTAD /$MAPbI_3$/TiO_2/FTO /Glass	Dissolution, adsorption, and precipitation	DMF	– 99.97	PbI_2	0 1	16.65 16.04	[153]
Ag/spiro-OMeTAD /$FAPbI_3$/SnO_2/TiO_2 /FTO/glass	Dissolution, adsorption, and precipitation	ethyl acetate, water	– 95	PbI_2	0 1	21.50 21.58	[166]
Cu/Cr/C_{60}BCP /$Cs_{0.1}FA_{0.9}PbI_3$ /PTAA/ITO/glass	Dissolution, adsorption, and precipitation	DMF	– 99.2	PbI_2	0 1	21.0 20.4	[140]
Au/spiro-OMeTAD /$MAPbBr_3$-doped $MAPbI_3$/SnO/ITO /Glass	Selective dissolution and liquefaction	THF	– 99.97	Liquefied perovskite	0 1 2	20.9 20.7 20.4	[167]
Carbon/$MAPbI_3$ /SnO_2/ITO/glass	Dissolution and evaporation	DMF, DMSO	–	PbI_2	0 1 5	16.29 15.30 12.10	[163]
Al/spiro-OMeTAD /$MAPbI_3$/TiO_2/ITO /glass	Hot aqueous extraction and precipitation	water	87 ± 11	PbI_2	–	–	[164]

additional 2D perovskite layers offers an alternative approach for passivation, retardation of charge recombination, and improved charge extraction. Encapsulation techniques are also crucial in isolating PSCs from external stimuli, further improving their stability and reducing their environmental impact. Moreover, the utilization of Pb-adsorbing materials in encapsulation has demonstrated significant potential for reducing toxic Pb leakage, furthering the environmental friendliness of PSCs and reinforcing their position as a promising future renewable energy technology. These advancements in stability enhancement and environmental impact reduction are vital for the successful commercialization of PSCs as clean and efficient energy sources. Continued research and development in these domains are crucial for the extensive integration of PSCs and their contribution to a more sustainable and eco-friendly energy future. Furthermore, the industrial development of PSCs necessitates a comprehensive understanding of degradation mechanisms, crucial for formulating efficient solutions to enhance the Power Conversion Efficiency (PCE) and stability of PSCs. Additionally, given the diverse applications of perovskite solar cells in various fields, further research is imperative to achieve efficiency and stability tailored for extreme environments such as outer space, underwater, indoor settings, stretchable conditions, and flexible environments.

5.2. In situ regeneration

The regeneration and self-healing techniques hold great promise in PSC lifetime extension and stability enhancement. Various methods, including immersion in MAI solution, thermal decomposition, and solid–liquid–solid phase transitions induced by methylamine gas, have been successfully used to rejuvenate degraded PSCs and restore their photovoltaic performance. Additionally, self-healing strategies that involve reversible perovskite decomposition–reconstruction and prevention of escaped decomposed species have demonstrated the ability to enhance stability and durability. The use of polymers as scaffolds, in encapsulation techniques, redox shuttles, and as self-healing polymers offers potential solutions for addressing mechanical stresses and restoring degraded PSCs to their original state. As PSC technology continues to advance, further research and development of regeneration and self-healing techniques are essential for the sustainability and long-term viability of PSCs. Continued efforts to optimize and evaluate the long-term effectiveness of these strategies is crucial for achieving commercial viability and widespread adoption of PSC technology. Moreover, exploring the integration of self-healing polymers into flexible PSCs can open new possibilities for durable and resilient photovoltaic devices, enabling them to withstand mechanical stresses without compromising their functionality. Owing to these advancements, PSCs have the potential to become clean and efficient energy sources, contributing to a greener more sustainable future. However, for practical applications, research in the field of in situ regeneration technology should be complemented by studies on the environmental impacts affecting recovery performance, the number of renewable cycles, and associated limiting factors.

5.3. Recycling of noble materials

Recycling strategies for TCO substrates and metal electrodes in PSCs are crucial for cost-effectiveness and sustainability. Various methods, such as solvent immersion and dry transfer processes, have shown promising results in recovering and reusing TCO substrates and metal electrodes, which can significantly reduce fabrication costs and minimize environmental impacts. The successful use of alternative solvents, such as alkaline and alkylamine solutions, further demonstrated the feasibility of

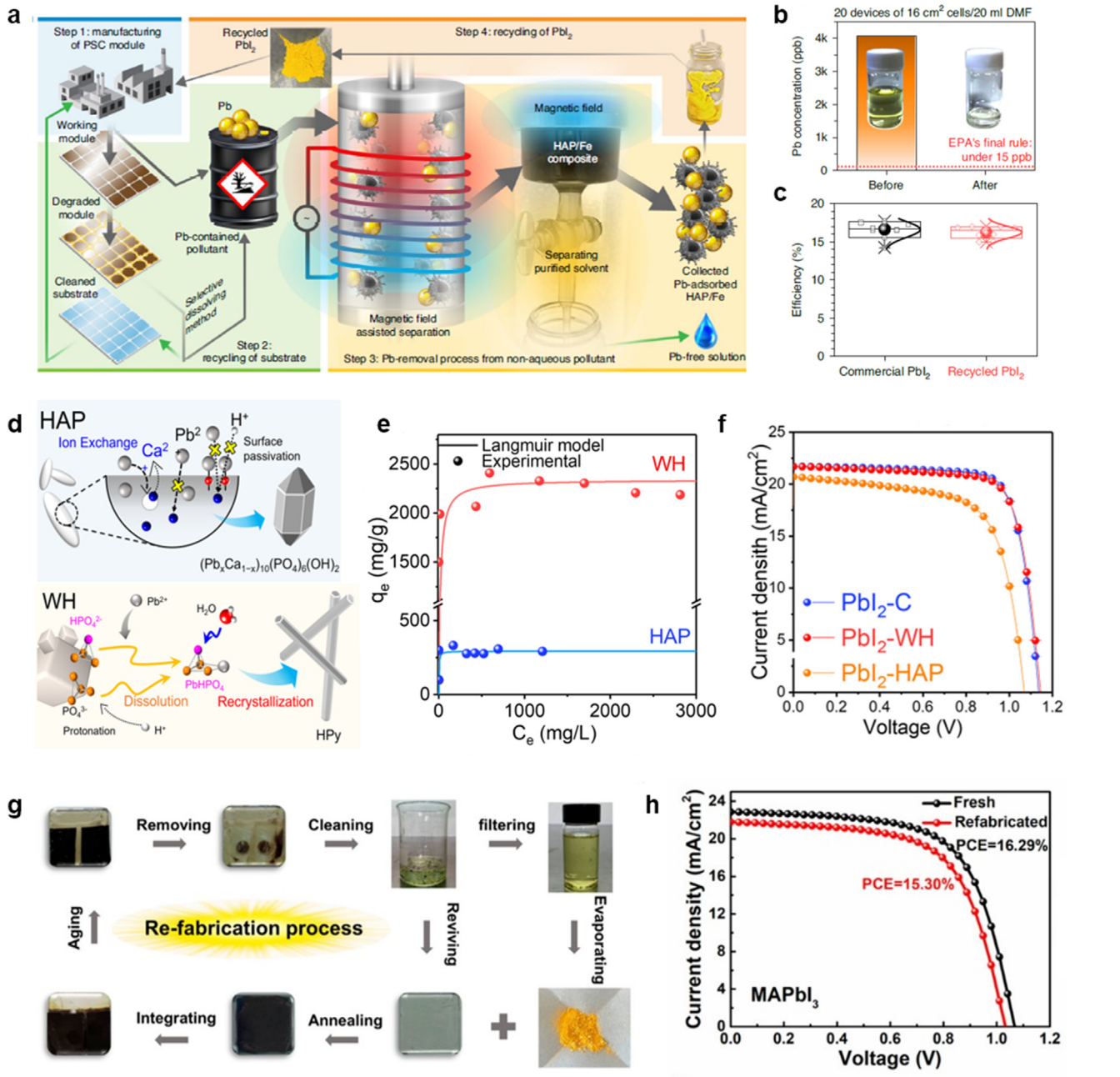

Fig. 13. (a) Schematic illustration of the Pb recycling process using HAP/Fe composite. (b) Pb concentration after Pb removal, and (c) PCE of PSCs fabricated with commercial PbI_2 and recycled PbI_2. Reproduced from Ref. [153]. Copyright 2020 Springer Nature. (d) Illustration of Pb adsorption mechanisms and (e) Langmuir isotherm of Pb removal by HAP and WH. (f) *J–V* curves of PSCs fabricated with commercial PbI_2 and PbI_2 recycled using WH and HAP. Reproduced from Ref. [158]. Copyright 2022 Wiley-VCH. (g) Fabrication process using recycled perovskite and ITO substrate, and (h) the PCE of fresh and refabricated PSCs. Reproduced from Ref. [163]. Copyright 2022 American Chemical Society.

recycling high-quality substrates with a photovoltaic performance comparable to that of fresh PSCs. However, challenges remain, particularly in the recycling of other materials; moreover, careful evaluation of the costs and environmental implications of the entire recycling process is necessary for the sustainable commercialization of PSCs. Recently, significant effort has been directed towards Si-PSC tandem solar cells to achieve high photovoltaic efficiency. Nonetheless, the distinct lifetimes of Si solar cells and PSCs pose significant challenges in maintaining continuous solar energy systems, making research on the recycling of PSCs an inevitable necessity. Therefore, continued research and development in recycling technologies and collaborative efforts between academia, research institutions, and industry players are essential for realizing the full potential of recycling in the PSC industry.

5.4. *Recycling of toxic materials*

Pb recycling from PSCs typically involves two main steps—perovskite layer dissolution and Pb compound extraction. Various solvents, including polar aprotic and deep eutectic solvents, have been employed for Pb recycling, leading to perovskite decomposition and Pb separation. Subsequently, methods such as electrochemical deposition, precipitation, and adsorption have been utilized to selectively extract Pb compounds from solutions or suspensions. Recycling of Pb compounds through these processes offers significant potential in enhancing the overall sustainability and reducing the environmental impact of PSCs. However, to fully realize these benefits, further advancements in solvent recycling and optimization of the extraction methods are required. Moreover, the

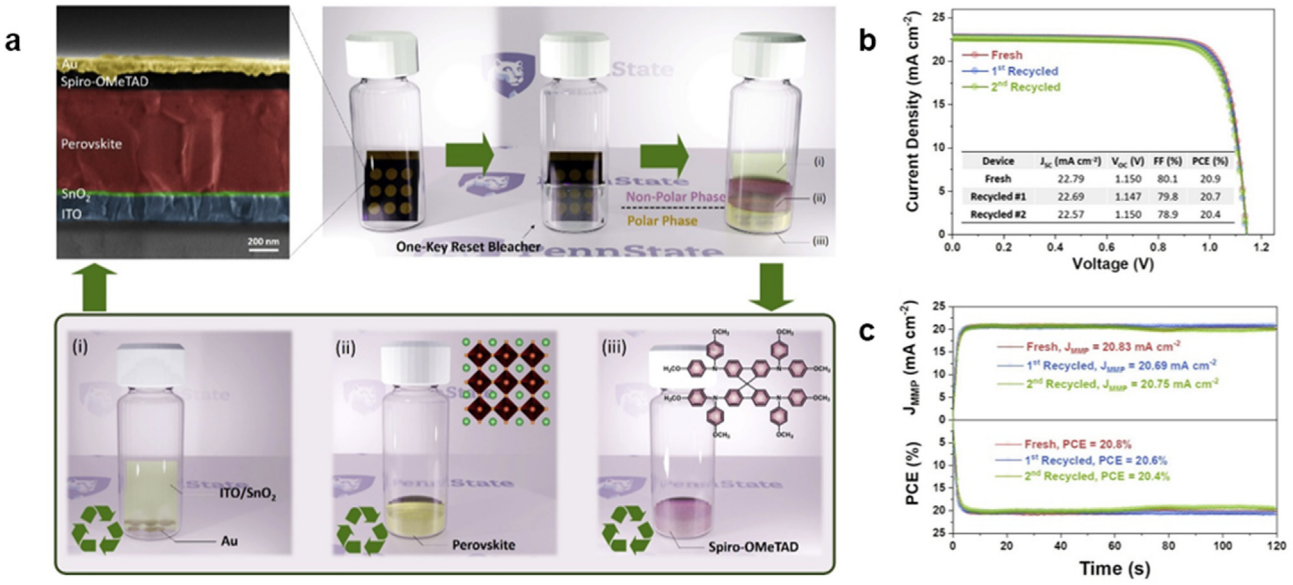

Fig. 14. (a) "One-key reset" recycling process using bleacher solution comprising non-polar and polar phases. (b) *J–V* characteristics and (c) steady-state current density and PCE for fresh, recycled, and twice-recycled PSCs. Reproduced from Ref. [167]. Copyright 2021 Elsevier.

recycling of toxic solvents used to fabricate PSCs presents a critical challenge that demands future attention. Although reports suggest the possibility of reusing solvents such as DMF and water, a comprehensive understanding of the maximum number of reuse cycles, associated costs, and environmental implications is crucial. Continued research efforts in this area are necessary to develop safe and efficient solvent-recycling methods that will ultimately reduce the overall environmental footprint of PSC production.

Author contributions

Hee Jung Kim: Conceptualization, Data curation, Investigation, Writing – original draft, Writing – review & editing. **Gill Sang Han:** Conceptualization, Supervision, Writing – review & editing. **Hyun Suk Jung:** Conceptualization, Funding acquisition, Supervision, Writing – review & editing.

Declaration of competing interest

The authors declare that they have no known competing financial interests or personal relationships that could have appeared to influence the work reported in this paper.

Acknowledgment

This paper was supported by SKKU Excellence in Research Award Research Fund, Sungkyunkwan University, 2023.

References

[1] H.-S. Kim, C.-R. Lee, J.-H. Im, K.-B. Lee, T. Moehl, A. Marchioro, S.-J. Moon, R. Humphry-Baker, J.-H. Yum, J.E. Moser, Lead iodide perovskite sensitized all-solid-state submicron thin film mesoscopic solar cell with efficiency exceeding 9%, Sci. Rep. 2 (2012) 591.
[2] Best Research-Cell Efficiency Chart. https://www.nrel.gov/pv/cell-efficiency.html.
[3] L. Meng, J. You, Y. Yang, Addressing the stability issue of perovskite solar cells for commercial applications, Nat. Commun. 9 (2018) 5265.
[4] G. Grancini, C. Roldan-Carmona, I. Zimmermann, E. Mosconi, X. Lee, D. Martineau, S. Narbey, F. Oswald, F. De Angelis, M. Graetzel, M.K. Nazeeruddin, One-Year stable perovskite solar cells by 2D/3D interface engineering, Nat. Commun. 8 (2017) 15684.
[5] P. Holzhey, M. Prettl, S. Collavini, N.L. Chang, M. Saliba, Toward commercialization with lightweight, flexible perovskite solar cells for residential photovoltaics, Joule 7 (2023) 257–271.
[6] L. Shi, M.P. Bucknall, T.L. Young, M. Zhang, L. Hu, J. Bing, D.S. Lee, J. Kim, T. Wu, N. Takamure, Gas chromatography–mass spectrometry analyses of encapsulated stable perovskite solar cells, Science 368 (2020) eaba2412.
[7] J.M. Kadro, A. Hagfeldt, The end-of-life of perovskite PV, Joule 1 (2017) 29–46.
[8] X. Tian, S.D. Stranks, F. You, Life cycle assessment of recycling strategies for perovskite photovoltaic modules, Nat. Sustain. 4 (2021) 821–829.
[9] M. Abdi-Jalebi, M.I. Dar, A. Sadhanala, S.P. Senanayak, M. Franckevičius, N. Arora, Y. Hu, M.K. Nazeeruddin, S.M. Zakeeruddin, M. Grätzel, Impact of monovalent cation halide additives on the structural and optoelectronic properties of $CH_3NH_3PbI_3$ perovskite, Adv. Energy Mater. 6 (2016) 1502472.
[10] M. Daboczi, S.R. Ratnasingham, L. Mohan, C. Pu, I. Hamilton, Y.-C. Chin, M.A. McLachlan, J.-S. Kim, Optimal interfacial band bending achieved by fine energy level tuning in mixed-halide perovskite solar cells, ACS Energy Lett. 6 (2021) 3970–3981.
[11] H.M. Ghaithan, Z.A. Alahmed, S.M. Qaid, A.S. Aldwayyan, First principle-based calculations of the optoelectronic features of 2 x 2 x 2 $CsPb(I_{1-x}Br_x)_3$ perovskite, Superlattices Microstruct. 140 (2020) 106474.
[12] H. Min, D.Y. Lee, J. Kim, G. Kim, K.S. Lee, J. Kim, M.J. Paik, Y.K. Kim, K.S. Kim, M.G. Kim, Perovskite solar cells with atomically coherent interlayers on SnO_2 electrodes, Nature 598 (2021) 444–450.
[13] Y. Zhao, F. Ma, Z. Qu, S. Yu, T. Shen, H.-X. Deng, X. Chu, X. Peng, Y. Yuan, X. Zhang, Inactive $(PbI_2)_2RbCl$ stabilizes perovskite films for efficient solar cells, Science 377 (2022) 531–534.
[14] H.J. Kim, O.Y. Gong, Y.J. Kim, G.W. Yoon, G.S. Han, H. Shin, H.S. Jung, Environmentally viable solvent management in perovskite solar cellrecycling process, ACS Energy Lett. 8 (2023) 4330–4337.
[15] J. Park, J. Kim, H.-S. Yun, M.J. Paik, E. Noh, H.J. Mun, M.G. Kim, T.J. Shin, S.I. Seok, Controlled growth of perovskite layers with volatile alkylammonium chlorides, Nature 616 (2023) 724–730.
[16] T. Bu, J. Li, F. Zheng, W. Chen, X. Wen, Z. Ku, Y. Peng, J. Zhong, Y.-B. Cheng, F. Huang, Universal passivation strategy to slot-die printed SnO_2 for hysteresis-free efficient flexible perovskite solar module, Nat. Commun. 9 (2018) 4609.
[17] Q. Lou, G. Lou, H. Guo, T. Sun, C. Wang, G. Chai, X. Chen, G. Yang, Y. Guo, H. Zhou, Enhanced efficiency and stability of n-i-p perovskite solar cells by incorporation of fluorinated graphene in the spiro-OMeTAD hole transport layer, Adv. Energy Mater. 12 (2022) 2201344.
[18] X. Li, W. Zhang, X. Guo, C. Lu, J. Wei, J. Fang, Constructing heterojunctions by surface sulfidation for efficient inverted perovskite solar cells, Science 375 (2022) 434–437.
[19] H. Chen, S. Teale, B. Chen, Y. Hou, L. Grater, T. Zhu, K. Bertens, S.M. Park, H.R. Atapattu, Y. Gao, Quantum-size-tuned heterostructures enable efficient and stable inverted perovskite solar cells, Nat. Photonics 16 (2022) 352–358.
[20] C. Li, X. Wang, E. Bi, F. Jiang, S.M. Park, Y. Li, L. Chen, Z. Wang, L. Zeng, H. Chen, Rational design of Lewis base molecules for stable and efficient inverted perovskite solar cells, Science 379 (2023) 690–694.
[21] H.S. Kim, J.Y. Seo, N.G. Park, Material and device stability in perovskite solar cells, ChemSusChem 9 (2016) 2528–2540.

[22] Y. Cheng, L. Ding, Pushing commercialization of perovskite solar cells by improving their intrinsic stability, Energy Environ. Sci. 14 (2021) 3233–3255.

[23] J. Zhu, Y. Qian, Z. Li, O.Y. Gong, Z. An, Q. Liu, J.H. Choi, H. Guo, P.J. Yoo, D.H. Kim, T.K. Ahn, G.S. Han, H.S. Jung, Defect healing in $FAPb(I_{1-x}Br_x)_3$ perovskites: multifunctional fluorinated sulfonate surfactant anchoring enables > 21% modules with improved operation stability, Adv. Energy Mater. 12 (2022).

[24] M. Wong-Stringer, O.S. Game, J.A. Smith, T.J. Routledge, B.A. Alqurashy, B.G. Freestone, A.J. Parnell, N. Vaenas, V. Kumar, M.O.A. Alawad, High-performance multilayer encapsulation for perovskite photovoltaics, Adv. Energy Mater. 8 (2018) 1801614–1806832.

[25] Y. Kato, L.K. Ono, M.V. Lee, S. Wang, S.R. Raga, Y. Qi, Silver iodide formation in methyl ammonium lead iodide perovskite solar cells with silver top electrodes, Adv. Mater. Interfaces 2 (2015) 1500195.

[26] H. Li, Z. Yan, M. Li, X. Wen, S. Deng, S. Liu, W.C. Choy, L. Li, M.-Y. Li, H. Lu, Probing the stability of perovskite solar cell under working condition through an ultra-thin silver electrode: beyond the halide ion diffusion and metal diffusion, Chem. Eng. J. 458 (2023) 141405.

[27] K. Domanski, J.-P. Correa-Baena, N. Mine, M.K. Nazeeruddin, A. Abate, M. Saliba, W. Tress, A. Hagfeldt, M. Grätzel, Not all that glitters is gold: metal-migration-induced degradation in perovskite solar cells, ACS Nano 10 (2016) 6306–6314.

[28] N.N. Shlenskaya, N.A. Belich, M. Grätzel, E.A. Goodilin, A.B. Tarasov, Light-induced reactivity of gold and hybrid perovskite as a new possible degradation mechanism in perovskite solar cells, J. Mater. Chem. A 6 (2018) 1780–1786.

[29] M. Stolterfoht, C.M. Wolff, J.A. Márquez, S. Zhang, C.J. Hages, D. Rothhardt, S. Albrecht, P.L. Burn, P. Meredith, T. Unold, Visualization and suppression of interfacial recombination for high-efficiency large-area pin perovskite solar cells, Nat. Energy 3 (2018) 847–854.

[30] L. Wang, G.-R. Li, Q. Zhao, X.-P. Gao, Non-precious transition metals as counter electrode of perovskite solar cells, Energy Stor. Mater. 7 (2017) 40–47.

[31] I. Jeong, H.J. Kim, B.-S. Lee, H.J. Son, J.Y. Kim, D.-K. Lee, D.-E. Kim, J. Lee, M.J. Ko, Highly efficient perovskite solar cells based on mechanically durable molybdenum cathode, Nano Energy 17 (2015) 131–139.

[32] W.Q. Wu, P.N. Rudd, Q. Wang, Z. Yang, J. Huang, Blading phase-pure formamidinium-alloyed perovskites for high-efficiency solar cells with low photovoltage deficit and improved stability, Adv. Mater. 32 (2020) 2000995.

[33] W.-q. Wu, P.N. Rudd, Z. Ni, C.H. Van Brackle, H. Wei, Q. Wang, B.R. Ecker, Y. Gao, J. Huang, Reducing surface halide deficiency for efficient and stable iodide-based perovskite solar cells, J. Am. Chem. Soc. 142 (2020) 3989–3996.

[34] F. Behrouznejad, S. Shahbazi, N. Taghavinia, H.-P. Wu, E.W.-G. Diau, A study on utilizing different metals as the back contact of $CH_3NH_3PbI_3$ perovskite solar cells, J. Mater. Chem. A 4 (2016) 13488–13498.

[35] Z. Xu, N. Li, X. Niu, H. Liu, G. Liu, Q. Chen, H. Zhou, Balancing energy-level difference for efficient nip perovskite solar cells with Cu electrode, Energy Mater. Adv. 2022 (2022) 9781073.

[36] J. Zhao, X. Zheng, Y. Deng, T. Li, Y. Shao, A. Gruverman, J. Shield, J. Huang, Is Cu a stable electrode material in hybrid perovskite solar cells for a 30-year lifetime? Energy Environ. Sci. 9 (2016) 3650–3656.

[37] D. Raptis, V. Stoichkov, S.M. Meroni, A. Pockett, C.A. Worsley, M. Carnie, D.A. Worsley, T. Watson, Enhancing fully printable mesoscopic perovskite solar cell performance using integrated metallic grids to improve carbon electrode conductivity, Curr. Appl. Phys. 20 (2020) 619–627.

[38] D. Bogachuk, B. Yang, J. Suo, D. Martineau, A. Verma, S. Narbey, M. Anaya, K. Frohna, T. Doherty, D. Müller, Perovskite solar cells with carbon-based electrodes–quantification of losses and strategies to overcome them, Adv. Energy Mater. 12 (2022) 2103128.

[39] M.K. Mohammed, High-performance hole conductor-free perovskite solar cell using a carbon nanotube counter electrode, RSC Adv. 10 (2020) 35831–35839.

[40] F. Bu, B. He, Y. Ding, X. Li, X. Sun, J. Duan, Y. Zhao, H. Chen, Q. Tang, Enhanced energy level alignment and hole extraction of carbon electrode for air-stable hole-transporting material-free $CsPbBr_3$ perovskite solar cells, Sol. Energy Mater. Sol. Cells 205 (2020) 110267.

[41] Q.-Q. Chu, Z. Sun, B. Ding, K.-s. Moon, G.-J. Yang, C.-P. Wong, Greatly enhanced power conversion efficiency of hole-transport-layer-free perovskite solar cell via coherent interfaces of perovskite and carbon layers, Nano Energy 77 (2020) 105110.

[42] L. Mi, Y. Zhang, T. Chen, E. Xu, Y. Jiang, Carbon electrode engineering for high efficiency all-inorganic perovskite solar cells, RSC Adv. 10 (2020) 12298–12303.

[43] R. Chen, Y. Feng, C. Zhang, M. Wang, L. Jing, C. Ma, J. Bian, Y. Shi, Carbon-based HTL-free modular perovskite solar cells with improved contact at perovskite/carbon interfaces, J. Mater. Chem. C 8 (2020) 9262–9270.

[44] T. Du, S. Qiu, X. Zhou, V.M. Le Corre, M. Wu, L. Dong, Z. Peng, Y. Zhao, D. Jang, E. Spiecker, Efficient, stable, and fully printed carbon-electrode perovskite solar cells enabled by hole-transporting bilayers, Joule 7 (2023) 1920–1937.

[45] F. Jiang, T. Liu, S. Zeng, Q. Zhao, X. Min, Z. Li, J. Tong, W. Meng, S. Xiong, Y. Zhou, Metal electrode–free perovskite solar cells with transfer-laminated conducting polymer electrode, Opt. Express 23 (2015) A83–A91.

[46] S. Wang, K. Hou, Y. Xing, Q. Dong, K. Wang, Y. Lv, Y. Shi, Flexibly assembled and readily detachable photovoltaics, Energy Environ. Sci. 10 (2017) 2117–2123.

[47] W.-C. Lai, K.-W. Lin, T.-F. Guo, P. Chen, Y.-Y. Liao, Efficient $CH_3NH_3PbI_3$ perovskite/fullerene planar heterojunction hybrid solar cells with oxidized Ni/Au/Cu transparent electrode, Appl. Phys. Lett. 112 (2018).

[48] E.M. Sanehira, B.J. Tremolet de Villers, P. Schulz, M.O. Reese, S. Ferrere, K. Zhu, L.Y. Lin, J.J. Berry, J.M. Luther, Influence of electrode interfaces on the stability of perovskite solar cells: reduced degradation using MoO_x/Al for hole collection, ACS Energy Lett. 1 (2016) 38–45.

[49] J. Wang, J. Li, Y. Zhou, C. Yu, Y. Hua, Y. Yu, R. Li, X. Lin, R. Chen, H. Wu, Tuning an electrode work function using organometallic complexes in inverted perovskite solar cells, J. Am. Chem. Soc. 143 (2021) 7759–7768.

[50] S. Yue, S. Lu, K. Ren, K. Liu, M. Azam, D. Cao, Z. Wang, Y. Lei, S. Qu, Z. Wang, Insights into the influence of work functions of cathodes on efficiencies of perovskite solar cells, Small 13 (2017) 1700007.

[51] Y. Wang, T. Gould, J.F. Dobson, H. Zhang, H. Yang, X. Yao, H. Zhao, Density functional theory analysis of structural and electronic properties of orthorhombic perovskite $CH_3NH_3PbI_3$, Phys. Chem. Chem. Phys. 16 (2014) 1424–1429.

[52] J. Carrillo, A. Guerrero, S. Rahimnejad, O. Almora, I. Zarazua, E. Mas-Marza, J. Bisquert, G. Garcia-Belmonte, Ionic reactivity at contacts and aging of methylammonium lead triiodide perovskite solar cells, Adv. Energy Mater. 6 (2016) 1502246.

[53] B. Niu, H. Wu, J. Yin, B. Wang, G. Wu, X. Kong, B. Yan, J. Yao, C.-Z. Li, H. Chen, Mitigating the lead leakage of high-performance perovskite solar cells via in situ polymerized networks, ACS Energy Lett. 6 (2021) 3443–3449.

[54] Y. Liang, P. Song, H. Tian, C. Tian, W. Tian, Z. Nan, Y. Cai, P. Yang, C. Sun, J. Chen, L. Xie, Q. Zhang, Z. Wei, Lead leakage preventable fullerene-porphyrin dyad for efficient and stable perovskite solar cells, Adv. Funct. Mater. 32 (2021).

[55] Y. Hu, Z. He, X. Jia, S. Zhang, Y. Tang, J. Wang, M. Wang, G. Sun, G. Yuan, L. Han, Dual functions of performance improvement and lead leakage mitigation of perovskite solar cells enabled by phenylbenzimidazole sulfonic acid, Small Methods 6 (2022) e2101257.

[56] J. Zhu, D.H. Kim, J.D. Kim, D.G. Lee, W.B. Kim, S.w. Chen, J.Y. Kim, J.M. Lee, H. Lee, G.S. Han, T.K. Ahn, H.S. Jung, All-in-one lewis base for enhanced precursor and device stability in highly efficient perovskite solar cells, ACS Energy Lett. 6 (2021) 3425–3434.

[57] X. Li, J. Du, H. Duan, H. Wang, L. Fan, Y. Sun, Y. Sui, J. Yang, F. Wang, L. Yang, Moisture-preventing $MAPbI_3$ solar cells with high photovoltaic performance via multiple ligand engineering, Nano Res. 15 (2021) 1375–1382.

[58] J. Wang, R. Zhang, H. Xu, Y. Chen, H. Zhang, N.-G. Park, Polyacrylic acid grafted carbon nanotubes for immobilization of lead(II) in perovskite solar cell, ACS Energy Lett. 7 (2022) 1577–1585.

[59] T. Wang, Y. Li, Q. Cao, J. Yang, B. Yang, X. Pu, Y. Zhang, J. Zhao, Y. Zhang, H. Chen, Deep defect passivation and shallow vacancy repair via an ionic silicone polymer toward highly stable inverted perovskite solar cells, Energy Environ. Sci. 15 (2022) 4414–4424.

[60] C. Qiu, J. Song, Y. Wu, X. Yin, L. Hu, Z. Su, Y. Jin, W. Wang, H. Wang, Z. Li, Defect passivation via a multifunctional organic additive toward efficient and stable inverted perovskite solar cells, Chem. Commun. 59 (2023) 6414–6417.

[61] H. Liang, W.D. Wang, S. Mai, X. Lv, J. Fang, J. Cao, Lead fixation by spider web-like porphyrin polymer for stable and clean perovskite solar cells, Chem. Eng. J. 429 (2022).

[62] Q. Cao, T. Wang, J. Yang, Y. Zhang, Y. Li, X. Pu, J. Zhao, H. Chen, X. Li, I. Tojiboyev, J. Chen, L. Etgar, X. Li, Environmental-friendly polymer for efficient and stable inverted perovskite solar cells with mitigating lead leakage, Adv. Funct. Mater. 32 (2022) 2201036.

[63] H. Bi, G. Han, M. Guo, C. Ding, H. Zou, Q. Shen, S. Hayase, W. Hou, Multistrategy preparation of efficient and stable environment-friendly lead-based perovskite solar cells, ACS Appl. Mater. Interfaces 14 (2022) 35513–35521.

[64] H. Zhang, K. Li, M. Sun, F. Wang, H. Wang, A.K.Y. Jen, Design of superhydrophobic surfaces for stable perovskite solar cells with reducing lead leakage, Adv. Energy Mater. 11 (2021) 2102281.

[65] Q. Wang, Z. Lin, J. Su, Y. Xu, X. Guo, Y. Li, M. Zhang, J. Zhang, J. Chang, Y. Hao, Dithiol surface treatment towards improved charge transfer dynamic and reduced lead leakage in lead halide perovskite solar cells, EcoMat 4 (2022) e12185.

[66] X. Meng, X. Hu, Y. Zhang, Z. Huang, Z. Xing, C. Gong, L. Rao, H. Wang, F. Wang, T. Hu, L. Tan, Y. Song, Y. Chen, A Biomimetic self-shield interface for flexible perovskite solar cells with negligible lead leakage, Adv. Funct. Mater. 31 (2021) 2106460.

[67] X. Zhu, H. Dong, J. Chen, J. Xu, Z. Li, F. Yuan, J. Dai, B. Jiao, X. Hou, J. Xi, Z. Wu, Photoinduced cross linkable polymerization of flexible perovskite solar cells and modules by incorporating benzyl acrylate, Adv. Funct. Mater. 32 (2022) 2202408.

[68] S. Wu, L. Liu, B. Zhang, Y. Gao, L. Shang, S. He, S. Li, P. Zhang, S. Chen, Y. Wang, Multifunctional two-dimensional benzodifuran-based polymer for eco-friendly perovskite solar cells featuring high stability, ACS Appl. Mater. Interfaces 14 (2022) 41389–41399.

[69] H. Guo, X. Yang, J. Zhu, Z. An, O.Y. Gong, Z. Li, P.J. Yoo, S. Kim, G.S. Han, H.S. Jung, Bifunctional modified biopolymer for highly efficient and stable perovskite solar cells and modules, Chem. Eng. J. 460 (2023) 141699.

[70] D. Xu, R. Mai, Y. Jiang, C. Chen, R. Wang, Z. Xu, K. Kempa, G. Zhou, J.-M. Liu, J. Gao, An internal encapsulating layer for efficient, stable, repairable and low-lead-leakage perovskite solar cells, Energy Environ. Sci. 15 (2022) 3891–3900.

[71] X. Zhu, S. Yang, Y. Cao, L. Duan, M. Du, J. Feng, Y. Jiao, X. Jiang, Y. Sun, H. Wang, S. Zuo, Y. Liu, S. Liu, Ionic-liquid-perovskite capping layer for stable 24.33%-efficient solar cell, Adv. Energy Mater. 12 (2021) 2103491.

[72] J.Y. Kim, G.S. Han, J.M. Lee, S. Mun, O.Y. Gong, C. Sohn, G. Park, I.S. Cho, Y. Kim, D.H. Kim, H.S. Jung, In situ formation of Imidazole-based 2D interlayer for efficient perovskite solar cells and modules, Int. J. Energy Res. 46 (2022) 15419–15427.

[73] C. Liu, Y. Yang, K. Rakstys, A. Mahata, M. Franckevicius, E. Mosconi, R. Skackauskaite, B. Ding, K.G. Brooks, O.J. Usiobo, J.N. Audinot, H. Kanda, S. Driukas, G. Kavaliauskaite, V. Gulbinas, M. Dessimoz, V. Getautis, F. De Angelis, Y. Ding, S. Dai, P.J. Dyson, M.K. Nazeeruddin, Tuning structural isomers of

phenylenediammonium to afford efficient and stable perovskite solar cells and modules, Nat. Commun. 12 (2021) 6394.
[74] F. Wang, X. Li, H. Duan, H. Wang, L. Fan, Y. Sun, Y. Sui, J. Yang, L. Yang, Toward efficient, moisture-resistant and lead-leakproofness perovskite solar cells: coordination-driven reconstructing homogeneous amorphous perovskitoid/crystalline perovskite photoabsorber, Chem. Eng. J. 428 (2022) 132528.
[75] D. Zhang, X. Wang, T. Tian, X. Xia, J. Duan, Z. Fan, F. Li, Multi-functional buried interface engineering derived from in-situ-formed 2D perovskites using π-conjugated liquid-crystalline molecule with aggregation-induced emission for efficient and stable NiO_x-based inverted perovskite solar cells, Chem. Eng. J. 469 (2023) 143789.
[76] D. Wei, F. Ma, R. Wang, S. Dou, P. Cui, H. Huang, J. Ji, E. Jia, X. Jia, S. Sajid, Ion-migration inhibition by the cation–π interaction in perovskite materials for efficient and stable perovskite solar cells, Adv. Mater. 30 (2018) 1707583.
[77] S. Kawachi, M. Atsumi, N. Saito, N. Ohashi, Y. Murakami, J.-i. Yamaura, Structural and thermal properties in formamidinium and Cs-mixed lead halides, J. Phys. Chem. Lett. 10 (2019) 6967–6972.
[78] G. Galeotti, F. De Marchi, E. Hamzehpoor, O. MacLean, M. Rajeswara Rao, Y. Chen, L.V. Besteiro, D. Dettmann, L. Ferrari, F. Frezza, Synthesis of mesoscale ordered two-dimensional π-conjugated polymers with semiconducting properties, Nat. Mater. 19 (2020) 874–880.
[79] S. Jhulki, J. Kim, I.-C. Hwang, G. Haider, J. Park, J.Y. Park, Y. Lee, W. Hwang, A.A. Dar, B. Dhara, Solution-processable, crystalline π-conjugated two-dimensional polymers with high charge carrier mobility, Chem 6 (2020) 2035–2045.
[80] L. Liang, H. Luo, J. Hu, H. Li, P. Gao, Efficient perovskite solar cells by reducing interface-mediated recombination: a bulky amine approach, Adv. Energy Mater. 10 (2020) 2000197.
[81] M.A. Mahmud, T. Duong, J. Peng, Y. Wu, H. Shen, D. Walter, H.T. Nguyen, N. Mozaffari, G.D. Tabi, K.R. Catchpole, Origin of efficiency and stability enhancement in high-performing mixed dimensional 2D-3D perovskite solar cells: a review, Adv. Funct. Mater. 32 (2022) 2009164.
[82] N. Rolston, K.A. Bush, A.D. Printz, A. Gold-Parker, Y. Ding, M.F. Toney, M.D. McGehee, R.H. Dauskardt, Engineering stress in perovskite solar cells to improve stability, Adv. Energy Mater. 8 (2018) 1802139.
[83] T. Liu, X. Zhao, X. Zhong, Q.C. Burlingame, A. Kahn, Y.-L. Loo, Improved absorber phase stability, performance, and lifetime in inorganic perovskite solar cells with alkyltrimethoxysilane strain-release layers at the perovskite/TiO_2 interface, ACS Energy Lett. 7 (2022) 3531–3538.
[84] H. Huang, H. Yan, M. Duan, J. Ji, X. Liu, H. Jiang, B. Liu, S. Sajid, P. Cui, Y. Li, TiO_2 surface oxygen vacancy passivation towards mitigated interfacial lattice distortion and efficient perovskite solar cell, Appl. Surf. Sci. 544 (2021) 148583.
[85] Q. Zhou, J. Duan, X. Yang, Y. Duan, Q. Tang, Interfacial strain release from the WS_2/$CsPbBr_3$ van der Waals heterostructure for 1.7 V voltage all-inorganic perovskite solar cells, Angew. Chem. Int. Ed. 59 (2020) 21997–22001.
[86] H. Guo, G.W. Yoon, Z.J. Li, Y. Yun, S. Lee, Y.H. Seo, N.J. Jeon, G.S. Han, H.S. Jung, In situ polymerization of cross-linked perovskite–polymer composites for highly stable and efficient perovskite solar cells, Adv. Energy Mater. 14 (2023) 2302743.
[87] T. Leijtens, G.E. Eperon, S. Pathak, A. Abate, M.M. Lee, H.J. Snaith, Overcoming ultraviolet light instability of sensitized TiO_2 with meso-superstructured organometal tri-halide perovskite solar cells, Nat. Commun. 4 (2013) 2885.
[88] J. Burschka, N. Pellet, S.-J. Moon, R. Humphry-Baker, P. Gao, M.K. Nazeeruddin, M. Grätzel, Sequential deposition as a route to high-performance perovskite-sensitized solar cells, Nature 499 (2013) 316–319.
[89] F. Matteocci, L. Cinà, E. Lamanna, S. Cacovich, G. Divitini, P.A. Midgley, C. Ducati, A. Di Carlo, Encapsulation for long-term stability enhancement of perovskite solar cells, Nano Energy 30 (2016) 162–172.
[90] G. Choudalakis, A. Gotsis, Free volume and mass transport in polymer nanocomposites, Curr. Opin. Colloid Interface Sci. 17 (2012) 132–140.
[91] J. Zhou, X. Tian, Y. Gao, S. Zhang, Y. Zhang, Z. Liu, W. Chen, Enhancing the stability of perovskite solar cells with a multilayer thin-film barrier, ACS Appl. Energy Mater. 6 (2023) 1413–1421.
[92] D. Kim, G.G. Jeon, J.H. Kim, J. Kim, N. Park, Design of a flexible thin-film encapsulant with sandwich structures of perhydropolysilazane layers, ACS Appl. Mater. Interfaces 14 (2022) 34678–34685.
[93] L. Sun, K. Uemura, T. Takahashi, T. Yoshida, Y. Suzuri, Interfacial engineering in solution processing of silicon-based hybrid multilayer for high performance thin film encapsulation, ACS Appl. Mater. Interfaces 11 (2019) 43425–43432.
[94] D.I. Kim, J.W. Lee, R.H. Jeong, J.W. Yang, S. Park, J.-H. Boo, Optical and water-repellent characteristics of an anti-reflection protection layer for perovskite solar cells fabricated in ambient air, Energy 210 (2020) 118582.
[95] R. Keshavarzi, N. Molabahrami, N. Afzali, M. Omrani, Improving efficiency and stability of carbon-based perovskite solar cells by a multifunctional triple-layer system: antireflective, UV-protective, superhydrophobic, and self-cleaning, Sol. RRL 4 (2020) 2000491.
[96] E. Cho, Y.Y. Kim, D.S. Ham, J.H. Lee, J.-S. Park, J. Seo, S.-J. Lee, Highly efficient and stable flexible perovskite solar cells enabled by using plasma-polymerized-fluorocarbon antireflection layer, Nano Energy 82 (2021) 105737. https://www.sciencedirect.com/journal/nano-energy/vol/82/suppl/C.
[97] Q. Wei, X. Huo, Q. Fu, T. Wang, H. Zhao, Y. Wang, J. Yang, S. Zhan, L. Zhou, S. Wang, An effective encapsulation for perovskite solar cells based on building-integrated photovoltaics, J. Mater. Chem. C 10 (2022) 8972–8978.
[98] S. Chen, Y. Deng, X. Xiao, S. Xu, P.N. Rudd, J. Huang, Preventing lead leakage with built-in resin layers for sustainable perovskite solar cells, Nat. Sustain. 4 (2021) 636–643.
[99] X. Li, F. Zhang, H. He, J.J. Berry, K. Zhu, T. Xu, On-device lead sequestration for perovskite solar cells, Nature 578 (2020) 555–558.
[100] Y. Jiang, L. Qiu, E.J. Juarez-Perez, L.K. Ono, Z. Hu, Z. Liu, Z. Wu, L. Meng, Q. Wang, Y. Qi, Reduction of lead leakage from damaged lead halide perovskite solar modules using self-healing polymer-based encapsulation, Nat. Energy 4 (2019) 585–593.
[101] L.R. Mendez, B.N. Breen, D. Cahen, Lead sequestration from halide perovskite solar cells with a low-cost thiol-containing encapsulant, ACS Appl. Mater. Interfaces 14 (2022) 29766–29772.
[102] X. Xiao, M. Wang, S. Chen, Y. Zhang, H. Gu, Y. Deng, G. Yang, C. Fei, B. Chen, Y. Lin, Lead-adsorbing ionogel-based encapsulation for impact-resistant, stable, and lead-safe perovskite modules, Sci. Adv. 7 (2021) eabi8249.
[103] S. Chen, Y. Deng, H. Gu, S. Xu, S. Wang, Z. Yu, V. Blum, J. Huang, Trapping lead in perovskite solar modules with abundant and low-cost cation-exchange resins, Nat. Energy 5 (2020) 1003–1011.
[104] Z. Li, X. Wu, B. Li, S. Zhang, D. Gao, Y. Liu, X. Li, N. Zhang, X. Hu, C. Zhi, A.K.Y. Jen, Z. Zhu, Sulfonated graphene aerogels enable safe-to-use flexible perovskite solar modules, Adv. Energy Mater. 12 (2021) 2103236.
[105] D.R. Ceratti, Y. Rakita, L. Cremonesi, R. Tenne, V. Kalchenko, M. Elbaum, D. Oron, M.A.C. Potenza, G. Hodes, D. Cahen, Self-healing inside $APbBr_3$ halide perovskite crystals, Adv. Mater. 30 (2018) 1706273.
[106] N. Phung, A. Al-Ashouri, S. Meloni, A. Mattoni, S. Albrecht, E.L. Unger, A. Merdasa, A. Abate, The role of grain boundaries on ionic defect migration in metal halide perovskites, Adv. Energy Mater. 10 (2020) 1903735.
[107] S.K. Gautam, M. Kim, D.R. Miquita, J.E. Bourée, B. Geffroy, O. Plantevin, Reversible photoinduced phase segregation and origin of long carrier lifetime in mixed-halide perovskite films, Adv. Funct. Mater. 30 (2020) 2002622.
[108] Y. Cheng, X. Liu, Z. Guan, M. Li, Z. Zeng, H.W. Li, S.W. Tsang, A.G. Aberle, F. Lin, Revealing the degradation and self-healing mechanisms in perovskite solar cells by sub-bandgap external quantum efficiency spectroscopy, Adv. Mater. 33 (2021) e2006170.
[109] W. Nie, J.-C. Blancon, A.J. Neukirch, K. Appavoo, H. Tsai, M. Chhowalla, M.A. Alam, M.Y. Sfeir, C. Katan, J. Even, Light-activated photocurrent degradation and self-healing in perovskite solar cells, Nat. Commun. 7 (2016) 11574.
[110] B. Jo, G.S. Han, H.M. Yu, J. Choi, J. Zhu, T.K. Ahn, G. Namkoong, H.S. Jung, Composites of cross-linked perovskite/polymer with sodium borate for efficient and stable perovskite solar cells, J. Mater. Chem. A 10 (2022) 14884–14893.
[111] Y. Zhao, J. Wei, H. Li, Y. Yan, W. Zhou, D. Yu, Q. Zhao, A polymer scaffold for self-healing perovskite solar cells, Nat. Commun. 7 (2016) 10228.
[112] Y. Niu, D. He, Z. Zhang, J. Zhu, T. Gavin, P. Falaras, L. Hu, Improved crystallinity and self-healing effects in perovskite solar cells via functional incorporation of polyvinylpyrrolidone, J. Energy Chem. 68 (2022) 12–18.
[113] Y. Lv, H. Zhang, R. Liu, Y. Sun, W. Huang, Composite encapsulation enabled superior comprehensive stability of perovskite solar cells, ACS Appl. Mater. Interfaces 12 (2020) 27277–27285.
[114] Q. Chang, F. Wang, W. Xu, A. Wang, Y. Liu, J. Wang, Y. Yun, S. Gao, K. Xiao, L. Zhang, L. Wang, J. Wang, W. Huang, T. Qin, Ferrocene-induced perpetual recovery on all elemental defects in perovskite solar cells, Angew. Chem. Int. Ed. 60 (2021) 25567–25574.
[115] L. Wang, H. Zhou, J. Hu, B. Huang, M. Sun, B. Dong, G. Zheng, Y. Huang, Y. Chen, L. Li, A Eu^{3+}-Eu^{2+} ion redox shuttle imparts operational durability to Pb-I perovskite solar cells, Science 363 (2019) 265–270.
[116] K. Zhang, Y. Deng, X. Shi, X. Li, D. Qi, B. Jiang, Y. Huang, Interface chelation induced by pyridine-based polymer for efficient and durable air-processed perovskite solar cells, Angew. Chem. Int. Ed. 61 (2022) e202112673.
[117] Y. Lan, Y. Wang, Y. Lai, Z. Cai, M. Tao, Y. Wang, M. Li, X. Dong, Y. Song, Thermally driven self-healing efficient flexible perovskite solar cells, Nano Energy 100 (2022) 107523.
[118] X. Meng, Z. Xing, X. Hu, Z. Huang, T. Hu, L. Tan, F. Li, Y. Chen, Stretchable perovskite solar cells with recoverable performance, Angew. Chem. Int. Ed. 59 (2020) 16602–16608.
[119] B.P. Finkenauer, Y. Gao, X. Wang, Y. Tian, Z. Wei, C. Zhu, D.J. Rokke, L. Jin, L. Meng, Y. Yang, Mechanically robust and self-healable perovskite solar cells, Cell Rep. Phys. Sci. 2 (2021) 100320.
[120] C. Eames, J.M. Frost, P.R.F. Barnes, B.C. O'Regan, A. Walsh, M.S. Islam, Ionic transport in hybrid lead iodide perovskite solar cells, Nat. Commun. 6 (2015) 7497.
[121] A. Ciccioli, A. Latini, Thermodynamics and the intrinsic stability of lead halide perovskites $CH_3NH_3PbX_3$, J. Phys. Chem. Lett. 9 (2018) 3756–3765.
[122] H. Luo, P. Li, J. Ma, L. Han, Y. Zhang, Y. Song, Sustainable Pb management in perovskite solar cells toward eco-friendly development, Adv. Energy Mater. 12 (2022) 2201242.
[123] R.K. Gunasekaran, D. Chinnadurai, A.R. Selvaraj, R. Rajendiran, K. Senthil, K. Prabakar, Revealing the self-degradation mechanisms in methylammonium lead iodide perovskites in dark and vacuum, ChemPhysChem 19 (2018) 1507–1513.
[124] S. Wang, Y. Jiang, E.J. Juarez-Perez, L.K. Ono, Y. Qi, Accelerated degradation of methylammonium lead iodide perovskites induced by exposure to iodine vapour, Nat. Energy 2 (2016) 16195.
[125] Y.-Y. Huang, G. Gollavelli, Y.-H. Chao, C.-S. Hsu, Rejuvenation of perovskite solar cells, J. Mater. Chem. C 4 (2016) 7595–7600.
[126] Q.-D. Dao, R. Tsuji, A. Fujii, M. Ozaki, Study on degradation mechanism of perovskite solar cell and their recovering effects by introducing CH_3NH_3I layers, Org. Electron. 43 (2017) 229–234.
[127] J. Xu, Z. Hu, L. Huang, X. Huang, X. Jia, J. Zhang, J. Zhang, Y. Zhu, In situ recycle of PbI_2 as a step towards sustainable perovskite solar cells, Prog. Photovolt. 25 (2017) 1022–1033.

[128] A.K. Jena, Y. Numata, M. Ikegami, T. Miyasaka, Role of spiro-OMeTAD in performance deterioration of perovskite solar cells at high temperature and reuse of the perovskite films to avoid Pb-waste, J. Mater. Chem. A 6 (2018) 2219–2230.
[129] L. Hong, Y. Hu, A. Mei, Y. Sheng, P. Jiang, C. Tian, Y. Rong, H. Han, Improvement and regeneration of perovskite solar cells via methylamine gas post-treatment, Adv. Funct. Mater. 27 (2017) 1703060.
[130] P. Chhillar, B.P. Dhamaniya, V. Dutta, S.K. Pathak, Recycling of perovskite films: route toward cost-efficient and environment-friendly perovskite technology, ACS Omega 4 (2019) 11880–11887.
[131] E.C. Directive, Directive 2012/19/EU of the european parliament and of the council of 4 July 2012 on waste electrical and electronic equipment, WEEE, Off. J. Eur. Union Law 197 (2012) 38–71.
[132] S. Maniarasu, T.B. Korukonda, V. Manjunath, E. Ramasamy, M. Ramesh, G. Veerappan, Recent advancement in metal cathode and hole-conductor-free perovskite solar cells for low-cost and high stability: a route towards commercialization, Renew. Sust. Energy Rev. 82 (2018) 845–857.
[133] F. Yang, J. Liu, Z. Lu, P. Dai, T. Nakamura, S. Wang, L. Chen, A. Wakamiya, K. Matsuda, Recycled utilization of a nanoporous Au electrode for reduced fabrication cost of perovskite solar cells, Adv. Sci. 7 (2020) 1902474.
[134] A. Binek, M.L. Petrus, N. Huber, H. Bristow, Y. Hu, T. Bein, P. Docampo, Recycling perovskite solar cells to avoid lead waste, ACS Appl. Mater. Interfaces 8 (2016) 12881–12886.
[135] J.M. Kadro, N. Pellet, F. Giordano, A. Ulianov, O. Müntener, J. Maier, M. Grätzel, A. Hagfeldt, Proof-of-concept for facile perovskite solar cell recycling, Energy Environ. Sci. 9 (2016) 3172–3179.
[136] B.J. Kim, D.H. Kim, S.L. Kwon, S.Y. Park, Z. Li, K. Zhu, H.S. Jung, Selective dissolution of halide perovskites as a step towards recycling solar cells, Nat. Commun. 7 (2016) 11735.
[137] L. Huang, Z. Hu, J. Xu, X. Sun, Y. Du, J. Ni, H. Cai, J. Li, J. Zhang, Efficient electron-transport layer-free planar perovskite solar cells via recycling the FTO/glass substrates from degraded devices, Sol. Energy Mater. Sol. Cells 152 (2016) 118–124.
[138] L. Huang, J. Xu, X. Sun, R. Xu, Y. Du, J. Ni, H. Cai, J. Li, Z. Hu, J. Zhang, New films on old substrates: toward green and sustainable energy production via recycling of functional components from degraded perovskite solar cells, ACS Sustain. Chem. Eng. 5 (2017) 3261–3269.
[139] B. Augustine, K. Remes, G.S. Lorite, J. Varghese, T. Fabritius, Recycling perovskite solar cells through inexpensive quality recovery and reuse of patterned indium tin oxide and substrates from expired devices by single solvent treatment, Sol. Energy Mater. Sol. Cells 194 (2019) 74–82.
[140] B. Chen, C. Fei, S. Chen, H. Gu, X. Xiao, J. Huang, Recycling lead and transparent conductors from perovskite solar modules, Nat. Commun. 12 (2021) 5859.
[141] X. Feng, S. Wang, Q. Guo, Y. Zhu, J. Xiu, L. Huang, Z. Tang, Z. He, Dialkylamines driven two-step recovery of NiO(x)/ITO substrates for high-reproducibility recycling of perovskite solar cells, J. Phys. Chem. Lett. 12 (2021) 4735–4741.
[142] X. Zhao, H. Shen, R. Sun, Q. Luo, X. Li, Y. Zhou, M. Tai, J. Li, Y. Gao, X. Li, H. Lin, Bending durable and recyclable mesostructured perovskite solar cells based on superaligned ZnO nanorod electrode, Sol. RRL 2 (2018) 1700194.
[143] N. Espinosa, L. Serrano-Luján, A. Urbina, F.C. Krebs, Solution and vapour deposited lead perovskite solar cells: ecotoxicity from a life cycle assessment perspective, Sol. Energy Mater. Sol. Cells 137 (2015) 303–310.
[144] I. Celik, Z. Song, A.J. Cimaroli, Y. Yan, M.J. Heben, D. Apul, Life cycle assessment (LCA) of perovskite PV cells projected from lab to fab, Sol. Energy Mater. Sol. Cells 156 (2016) 157–169.
[145] P. Billen, E. Leccisi, S. Dastidar, S. Li, L. Lobaton, S. Spatari, A.T. Fafarman, V.M. Fthenakis, J.B. Baxter, Comparative evaluation of lead emissions and toxicity potential in the life cycle of lead halide perovskite photovoltaics, Energy 166 (2019) 1089–1096.
[146] K. Nishimura, M.A. Kamarudin, D. Hirotani, K. Hamada, Q. Shen, S. Iikubo, T. Minemoto, K. Yoshino, S. Hayase, Lead-free tin-halide perovskite solar cells with 13% efficiency, Nano Energy 74 (2020) 104858.
[147] C. Wang, Y. Zhang, F. Gu, Z. Zhao, H. Li, H. Jiang, Z. Bian, Z. Liu, Illumination durability and high-efficiency Sn-based perovskite solar cell under coordinated control of phenylhydrazine and halogen ions, Matter 4 (2021) 709–721.
[148] B.B. Yu, Z. Chen, Y. Zhu, Y. Wang, B. Han, G. Chen, X. Zhang, Z. Du, Z. He, Heterogeneous 2D/3D tin-halides perovskite solar cells with certified conversion efficiency breaking 14%, Adv. Mater. 33 (2021) 2102055.
[149] L. Serrano-Lujan, N. Espinosa, T.T. Larsen-Olsen, J. Abad, A. Urbina, F.C. Krebs, Tin-and lead-based perovskite solar cells under scrutiny: an environmental perspective, Adv. Energy Mater. 5 (2015) 1501119.
[150] G. Schileo, G. Grancini, Lead or no lead? Availability, toxicity, sustainability and environmental impact of lead-free perovskite solar cells, J. Mater. Chem. C 9 (2021) 67–76.
[151] A. Babayigit, D. Duy Thanh, A. Ethirajan, J. Manca, M. Muller, H.-G. Boyen, B. Conings, Assessing the toxicity of Pb-and Sn-based perovskite solar cells in model organism Danio rerio, Sci. Rep. 6 (2016) 18721.
[152] S. Zhang, L. Shen, M. Huang, Y. Yu, L. Lei, J. Shao, Q. Zhao, Z. Wu, J. Wang, S. Yang, Cyclic utilization of lead in carbon-based perovskite solar cells, ACS Sustain. Chem. Eng. 6 (2018) 7558–7564.
[153] S.Y. Park, J.-S. Park, B.J. Kim, H. Lee, A. Walsh, K. Zhu, D.H. Kim, H.S. Jung, Sustainable lead management in halide perovskite solar cells, Nat. Sustain. 3 (2020) 1044–1051.
[154] H.J. Kim, J.M. Lee, J.H. Choi, D.H. Kim, G.S. Han, H.S. Jung, Synthesis and adsorption properties of gelatin-conjugated hematite (alpha-Fe_2O_3) nanoparticles for lead removal from wastewater, J. Hazard. Mater. 416 (2021) 125696.
[155] N.G. Mostafa, A.F. Yunnus, A. Elawwad, Adsorption of Pb (II) from water onto ZnO, TiO_2, and Al_2O_3: process study, adsorption behaviour, and thermodynamics, Adsorp. Sci. Technol. 2022 (2022).
[156] M. Vesali-Naseh, M.R. Vesali Naseh, P. Ameri, Adsorption of Pb (II) ions from aqueous solutions using carbon nanotubes: a systematic review, J. Clean. Prod. 291 (2021) 125917.
[157] E. Asuquo, A. Martin, P. Nzerem, F. Siperstein, X. Fan, Adsorption of Cd(II) and Pb(II) ions from aqueous solutions using mesoporous activated carbon adsorbent: equilibrium, kinetics and characterisation studies, J. Environ. Chem. Eng. 5 (2017) 679–698.
[158] J.S. Hong, H.J. Kim, C.H. Sohn, O.Y. Gong, J.H. Choi, K.H. Cho, G.S. Han, K.T. Nam, H.S. Jung, High-throughput Pb recycling for perovskite solar cells using biomimetic whitlockite, Energy Environ. Mater. 6 (2022) e12374.
[159] B. Sandrine, N. Ange, B.A. Didier, C. Eric, S. Patrick, Removal of aqueous lead ions by hydroxyapatites: equilibria and kinetic processes, J. Hazard. Mater. 139 (2007) 443–446.
[160] S. Elfeghe, Q. Sheng, Y. Zhang, Separation of lead and copper ions in acidic media using an ion-exchange resin with a thiourea functional group, ACS Omega 7 (2022) 13042–13049.
[161] C.G. Poll, G.W. Nelson, D.M. Pickup, A.V. Chadwick, D.J. Riley, D.J. Payne, Electrochemical recycling of lead from hybrid organic–inorganic perovskites using deep eutectic solvents, Green Chem. 18 (2016) 2946–2955.
[162] H. Wang, X. Chen, X. Li, J. Qu, H. Xie, S. Gao, D. Wang, H. Yin, Recovery of lead and iodine from spent perovskite solar cells in molten salt, Chem. Eng. J. 447 (2022) 137498.
[163] F. Deng, S. Li, X. Sun, H. Li, X. Tao, Full life-cycle lead management and recycling transparent conductors for low-cost perovskite solar cell, ACS Appl. Mater. Interfaces 14 (2022) 52163–52172.
[164] F. Schmidt, M. Amrein, S. Hedwig, M. Kober-Czerny, A. Paracchino, V. Holappa, R. Suhonen, A. Schaffer, E.C. Constable, H.J. Snaith, M. Lenz, Organic solvent free PbI_2 recycling from perovskite solar cells using hot water, J. Hazard. Mater. 447 (2023) 130829.
[165] X. Feng, Q. Guo, J. Xiu, Z. Ying, K.W. Ng, L. Huang, S. Wang, H. Pan, Z. Tang, Z. He, Close-loop recycling of perovskite solar cells through dissolution-recrystallization of perovskite by butylamine, Cell Rep. Phys. Sci. 2 (2021) 100341.
[166] M. Ren, Y. Miao, T. Zhang, Z. Qin, Y. Chen, N. Wei, X. Qian, T. Wang, Y. Zhao, Lead stabilization and iodine recycling of lead halide perovskite solar cells, ACS Sustain. Chem. Eng. 9 (2021) 16519–16525.
[167] K. Wang, T. Ye, X. Huang, Y. Hou, J. Yoon, D. Yang, X. Hu, X. Jiang, C. Wu, G. Zhou, S. Priya, "One-key-reset" recycling of whole perovskite solar cell, Matter 4 (2021) 2522–2541.
[168] D. Prat, J. Hayler, A. Wells, A survey of solvent selection guides, Green Chem. 16 (2014) 4546–4551.